THESIS

PROGRESS TOWARD A CLONEABLE BISMUTH NANOPARTICLE

Submitted by

Courtney Solomon

Department of Chemistry

In partial fulfillment of the requirements

For The Degree of Master of Science

Colorado State University

Fort Collins, Colorado

Summer 2025

Master's Committee:

Advisor: Chris Ackerson

Chris Snow
Susan Tsunoda

ABSTRACT

PROGRESS TOWARD A CLONEABLE BISMUTH NANOPARTICLE

Electron microscopy (EM) is a technique that obtains high resolution biological images. However, a major limitation is inadequate contrast between a protein of interest and the surrounding cellular background. To overcome this challenge, the Ackerson lab has developed a cloneable nanoparticles (cNPs) which are described as inorganic particle enzymatic synthesized using a metal reducing enzymes. These electron dense nanoparticles serve as a contrast marker, enhancing the contrast between a protein of interest and the cellular background.

The focus of my thesis is to create a small compact bismuth cNPs to improve contrast labelling in EM.

The first chapter provides an overview of current biological imaging and introduces how cloneable nanoparticles have promising application as a contrast marker. It reviews the role of essential intracellular metals and details the development of a cloneable selenium nanoparticle made from a metal reducing enzyme, Glutathione Reductase-Like Metalloid Reductase (GRLMR), which reduces selenite to form zero valance selenium. This chapter concludes by outlining the advantages of using bismuth as a contrasting marker.

The second chapter discusses the background of arsenate reductase (ArsC), which natively reduces arsenate to arsenite. Given the chemical and structural properties of arsenite and bismuth, I hypothesized that ArsC may be capable of reducing bismuth(III) glutathione. This hypothesis was tested through enzymatic activity assays and by observing particle formation using analytical techniques to determine whether ArsC can reduce $Bi(GSH)_3$.

The third chapter explores how a directed evolution approach enhances ArsC's selectivity towards reducing $Bi(GSH)_3$. I generated a random mutagenesis library of ArsC variants, with the next step focusing on screening or selecting for variants that exhibit improved activity towards $Bi(GSH)_3$.

ACKNOWLEDGEMENTS

I would like to thank my advisor, Dr. Chris Ackerson, for giving me the opportunity to work in his laboratory, first as a summer intern when I was an undergraduate and then in my master's program. His mentorship not only introduced me to the field of chemical biology but also helped shape my interest in it. I am deeply grateful for his continued support throughout my time at Colorado State University.

I want to extend my thanks to Rachel Cohen for her time, thoughtful feedback, and collaborative work on this project. Rachel has influenced my laboratory skills and scientific thinking. A special thanks to Tony Tien and Taylor Tomalinas for their expertise and assistance in imaging my samples. I would also like to thank the rest of the Ackerson lab for their assistance with this project.

Finally, I would like to thank my thesis committee Dr. Chris Snow and Dr. Susan Tsunoda for their time and their review of my thesis.

TABLE OF CONTENTS

CHAPTER 1: INTRODUCTION

1.1 Biological Imaging

Understanding protein function requires the study of its structure. Electron microscopy (EM) is a high resolution imaging technique that enables direct observation of molecular structures at atomic resolutions. However, most cellular components are primarily composed of the same elements (i.e., C, O, N, S, and P), which makes it difficult to distinguish a protein of interest from the complex cellular environment.[1] EM, like other biological imaging modalities relies on contrast markers to observe specific proteins of interest in the complex cellular environment. With a contrast marker, it becomes possible to observe a protein of interest in its native environment. A contrast marker should minimally perturb the native protein function.

In fluorescence imaging, cloneable contrast markers, exemplified by green fluorescence protein (GFP), are commonly used to locate proteins of interest. GFP and its variants are widely used because of their ability to be easily concatenated with any protein of interest in a variety of systems.[2] Fluorescent labelling can locate an area of interest, this has revolutionized our understanding of cellular structure and function.[3] However, fluorescent microscopy is fundamentally limited by the diffraction of light used.[4-6] Ultimately, fluorescent labelling cannot directly observe macromolecular structures even at superresolution techniques.

To overcome this problem, intracellular small electron-dense tag that do not perturb the protein's function and can effectively provide precise localization and structural information of proteins. Several contrasting tools are currently available (immunolabelling, genetically encoded multimeric particles, DNA origami, etc.), which are effective in specific applications. However,

more research is still needed to find a robust labelling method suitable for a broad range of biological questions.

Cloneable nanoparticles (cNPs) have promising potential as a broadly applicable labelling method. The Ackerson lab defines a cloneable nanoparticle (cNP) as inorganic particles enzymatically synthesized by metal reducing enzymes (i.e., protein precursors), which are genetically encoded in the host organism (Figure 1).[9] The properties of the nanoparticle are controlled by the protein precursor. By fusing an electron dense cNPs to a protein of interest, it becomes possible to visualize and locate the protein of interest from the biological environment. Since the inorganic nanoparticle is composed of more electron dense metal(loid) atoms, it appears much different than the surrounding cellular background enabling the protein of interest to be visualized by proxy.

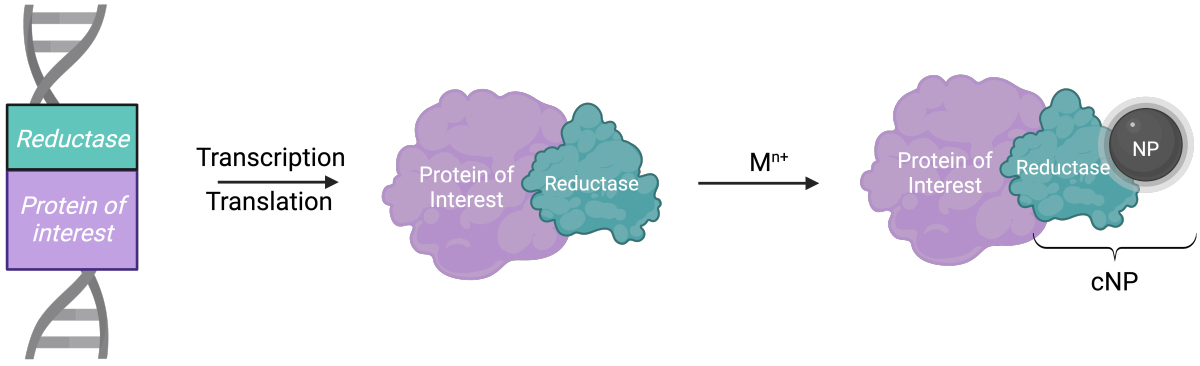

Figure 1: Schematic of cloneable nanoparticles (cNP) system. A genetically encoded metal reductase (protein precursor) is fused to a protein of interest. Once expressed, the metal reductase reduces a metal salt into an inorganic nanoparticle.

1.2 Intracellular Metals

Metals play a critical role in many biological processes.[10] For example, essential metals are necessary micronutrients that help the growth and development of an organism (Se, Cu, Fe, Mn, Ni, Zn, etc.).[11] However, at a certain concentration, metals become toxic regardless of their

role in the cell.[8-12] Cells tightly regulate essential metals within the cell to ensure they do not reach the toxic level.[11–13] Cells mitigate toxicity in a lot of different ways to reduce the toxic metal. One way cells can do this is by forming nanoparticles to reduce the toxicity of a soluble ion present in the cell. By forming nanoparticles, it reduces the toxicity in the cell and allows a less toxic metal(loid) to be present.

1.3 Current cNP Platform

Selenium is an essential nutrient that plays a role in immune function and protects against oxidative stress.[14–16] Specifically, in *Escherichia coli* (*E. coli)* selenium helps with bacteria growth and host immune response. Selenoproteins oxidoreductase and selenocysteine (i.e., the 21st amino acid that contains selenium) regulate the redox balance of selenium levels in the cell to prevent toxic levels from occurring.[16] One of the selenoproteins that are a critical precursor for DNA replication is thioredoxin reductase, which redox-active dithiol and disulfide in the active site. One of the major selenium metabolites is selenodiglutathione which forms a covalent molecule between selenite and glutathione (GS-Se-GS).[17]

The Ackerson lab discovered Glutathione Reductase-Like Metalloid Reductase (GRLMR) which was isolated from the roots of the selenium hyperaccumulating bacterium *Pseudomonas moraviensis stanleyae* (Figure 2).[13,18] The bacteria (*Pseudomonas moraviensis stanleyae)* has tolerance to normally lethal concentrations of selenium which is due to GRLMR reducing selenodiglutathione to zerovalent selenium forming an intracellular nanoparticle. When this enzyme is transformed (i.e., uptake into naked DNA) into *E. coli*, the same increase in selenium tolerance is observed.

GRLMR reduces selenodiglutathione (GS-Se-SG) to a zerovalent selenium nanoparticle.[19] This enzyme also shows low activity towards other selenosubstrates including

selenite and selenate.[19] A directed evolution experiment was successfully done, a GRLMR variant prefer a selenite substrate. GRLMR uses nicotinamide adenine dinucleotide phosphate hydrogen (NADPH) as an electron donor to reduce soluble selenium salts precursors, selenite (SeO_3^{2-}), into a zerovalent insoluble selenium cNPs (Figure 2).[9,20]

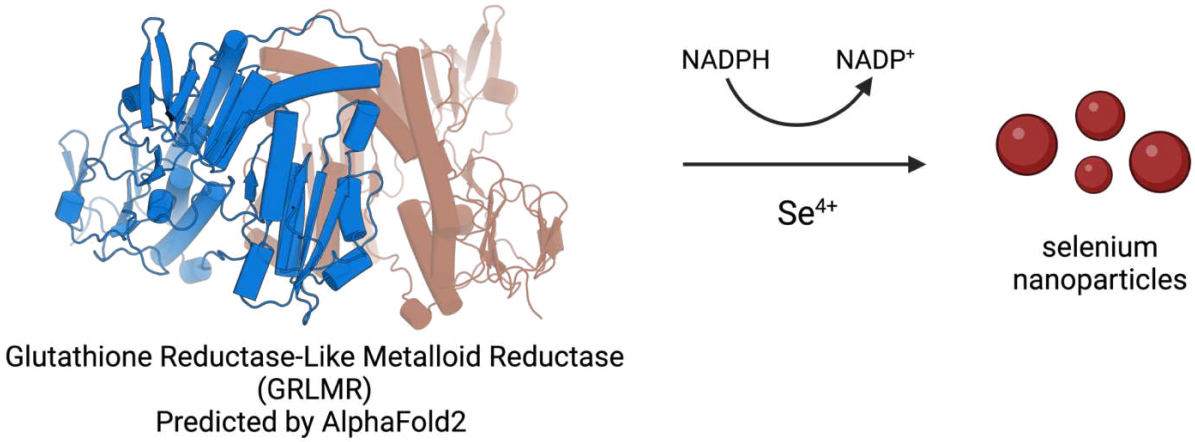

Figure 2: Schematic of selenium nanoparticle. Glutathione Reductase-Like Metalloid Reductase wild-type (predicted by AlphaFold2) in the formation of selenium nanoparticles

Selenium nanoparticles have successfully been observed in EM. However, due to the large size of GRLMR (100 kDa) and homodimer nature, this could pose challenges as a contrasting tag. Developing a small and compact cNP system could create a nonperturbed environment.

1.3 Ideal Contrasting Marker

Bismuth is the heaviest (i.e., highest atomic number) non-radioactive metal, making it an ideal candidate for generating small electron-rich cNPs.[21,22] Additionally, bismuth is generally considered biocompatible, classified as a non-toxic and non-carcinogenic metalloid, unlike many other heavy metals.[23]

In biological systems, bismuth predominantly exists in its trivalent oxidation state, bismuth(III). It exhibits a strong affinity toward thiols, particularly glutathione, which is a major antioxidant involved in metal detoxification. Given the high intracellular concentration of free glutathione, bismuth(III) could readily form a bismuth(III) glutathione, $Bi(GSH)_3$, complex.[24] However, research on this complex remains limited.

Enzymes can interact with different substrates that share similar chemistry. This has been demonstrated by GRLMR, which exhibits substrate promiscuity of different selenosubstrates. A similar approach can be applied to an enzymatical synthesis of a bismuth nanoparticle by utilizing an enzyme that natively reduces a pnictogen (i.e., group 15 element) substrate. We have identified an enzyme, arsenate reductase, as a potential candidate for bismuth cloneable nanoparticles. Through a directed evolution approach, mutations in the enzyme could improve specificity towards a bismuth reduction.

Specific Aims:

(1) Evaluate ArsC as a candidate for a cloneable bismuth NP

(2) Design a directed evolution experiment to evolve ArsC for more selective bismuth NP production

CHAPTER 2: ARSENATE REDUCTASE

2.1 Arsenicals

Arsenic is a ubiquitous, highly toxic metalloid and can lead to severe health conditions, such as cancer (i.e., lung, bladder, skin, kidney, liver, and/or prostate cancer).[25,26] Arsenic toxicity is attributed to its high affinity for thiol groups in proteins or in glutathione, which are abundant in most cells. This interaction can disrupt native protein function.[27]

Arsenate, As(V), shares structural and chemical similarities with phosphate(V), allowing arsenate to enter the cells via the phosphate transporters.[25,28] When intracellular arsenate levels get too high, a cell response is sent to start a detoxification process reducing arsenate to arsenite, As(III), which is transported out of the cell via the ArsA and ArsB pump. This detoxification is done through the *ars* operon.

There are five different genes that are encoded in the *E. coli* plasmid R773 *ars* operon arsRDABC which contribute to the detoxification of arsenicals (

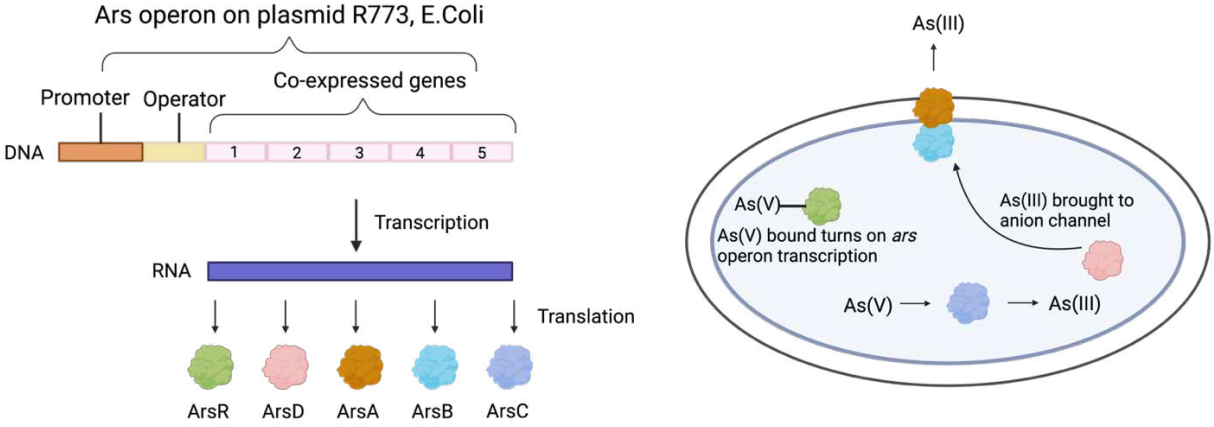

Figure ***3***). ArsR acts as a regulatory protein which controls the expression of the *ars* operon. In the presence of arsenate, it binds to ArsR causing a conformational change to occur and the ArsR dissociates from the DNA operator sequence, causing the *ars* operon to activate the

transcription.[27,29] Once transcription occurs and the genes are translated, ArsC reduces arsenate to arsenite, which is then transferred by ArsD to the ArsA and ArsB pump out of the cell (

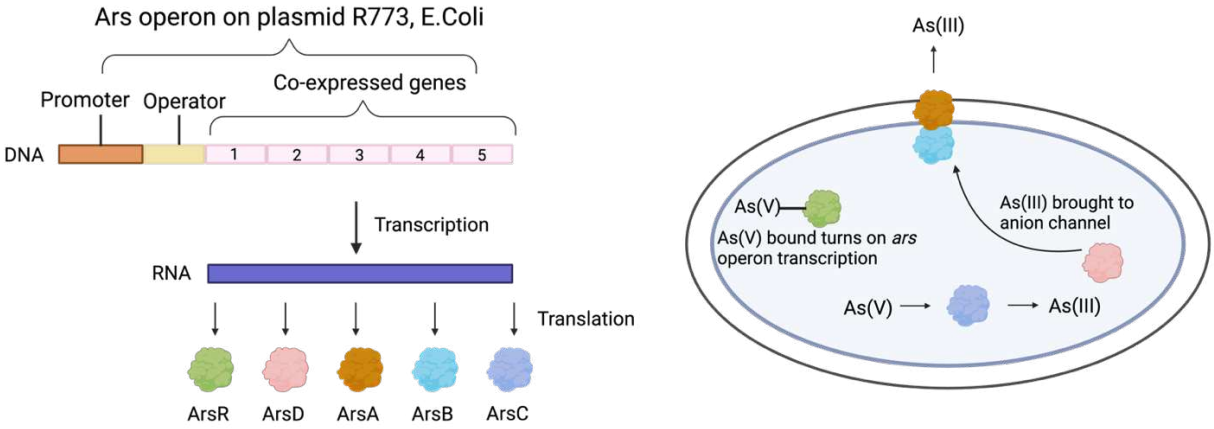

Figure *3*). If arsenite, As(III), is not removed from the cell, it can bind to cysteine and histidine residues in proteins and disturb enzymatic functions causing cellular damage.[30,31] ArsC is the enzyme that is responsible for the reduction of arsenate and is of particular interest to investigate whether a similar redox mechanism could occur for a Bi(III) reduction.

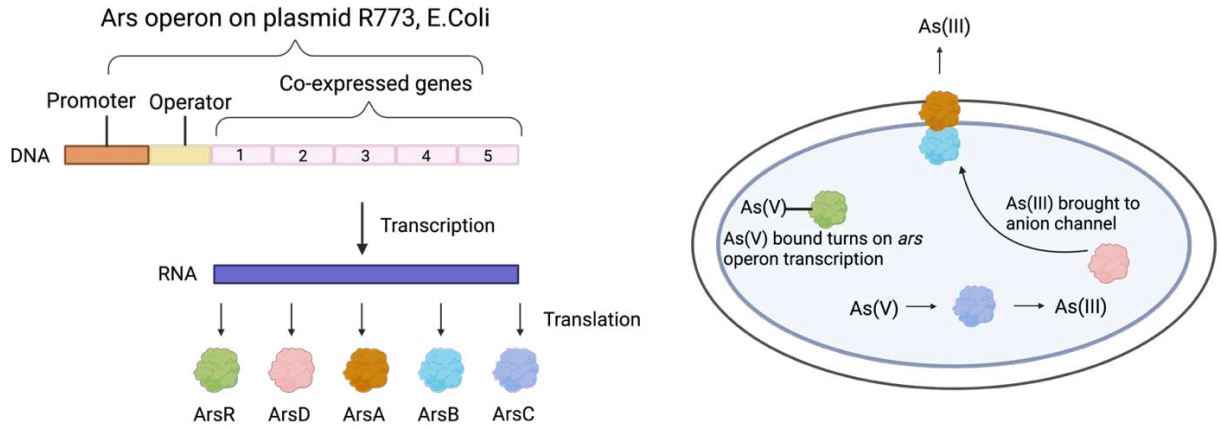

Figure 3: Mechanism of *ars operon*. In the presence of arsenate, five genes are co-expressed in this operon which reduces to arsenite which is then exported out of cell.

2.2 Arsenate reductase

The mechanism for arsenate reductase (ArsC) is not well understood, it is hypothesized that ArsC a small 16 kDa enzyme utilizes glutathione and glutaredoxin2 as an electron donor to natively reduce intracellular arsenate to arsenite via a two-electron transfer (

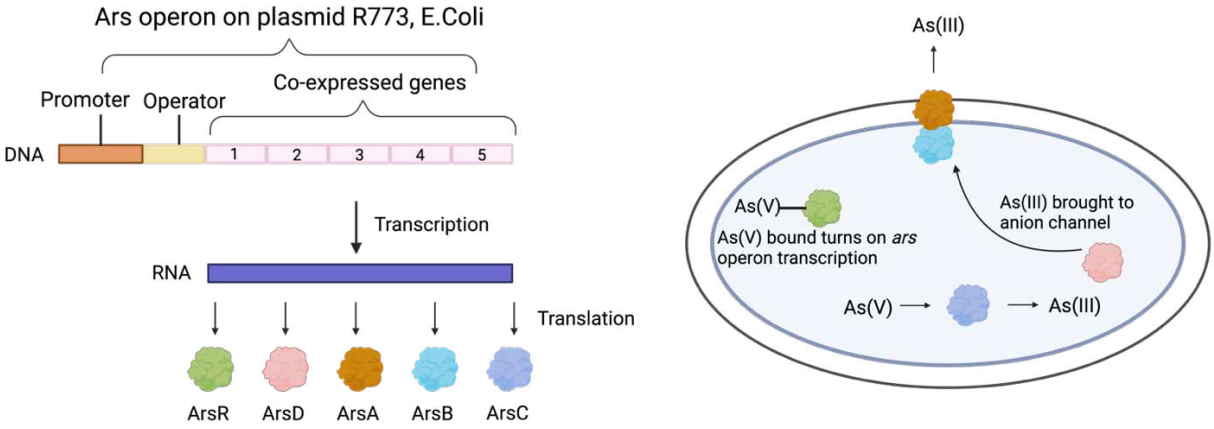

Figure ***3***, Figure 4).[32–35] The reduced arsenite is pumped out of the cell via the arsenite pathway (i.e., ArsA and ArsB) (

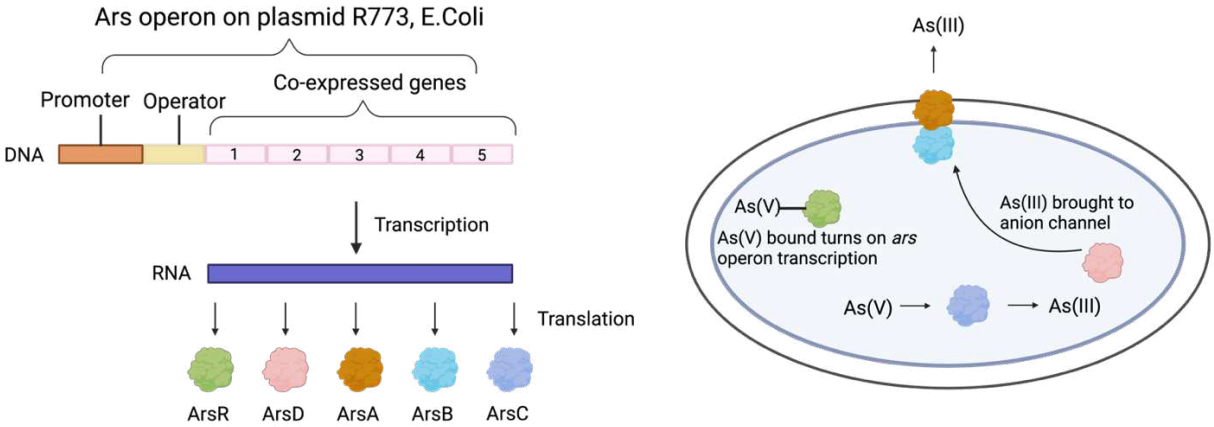

Figure ***3***).

The function of glutaredoxin2 (28 kDa) remains unknown but studies have reported that this enzyme acts as an electron donor for the reduction of arsenate by ArsC.[36] Although a detailed mechanism of glutaredoxin2 is not well understood, studies suggest that both cysteine residues are required for protein disulfide reduction to occur.[36]

While the exact catalytic mechanism of ArsC remains unclear, computational models have predicted the reduction mechanism (Figure 4).[30,34,36] It is predicted that the cysteine residue on ArsC does a nucleophilic attack on arsenate, forming an enzyme-substrate complex (seen as 1 in Figure 4).[31] Because arsenate interacts strongly with thiols groups, glutathione binds to the enzyme-substrate intermediate, releasing a hydroxyl group from the arsenate complex (seen as 2 in Figure 4). When glutaredoxin2 is reduced from NADPH, glutaredoxin2 grabs the thiol group on the intermediate complex (seen as 3 in Figure 4). Enzyme-substrate complex undergoes protonation, removing a free water molecule resulting in the enzyme-substrate intermediate breaking its bond, resulting in the formation of arsenite (seen as 4 in Figure 4).[34,36,37]

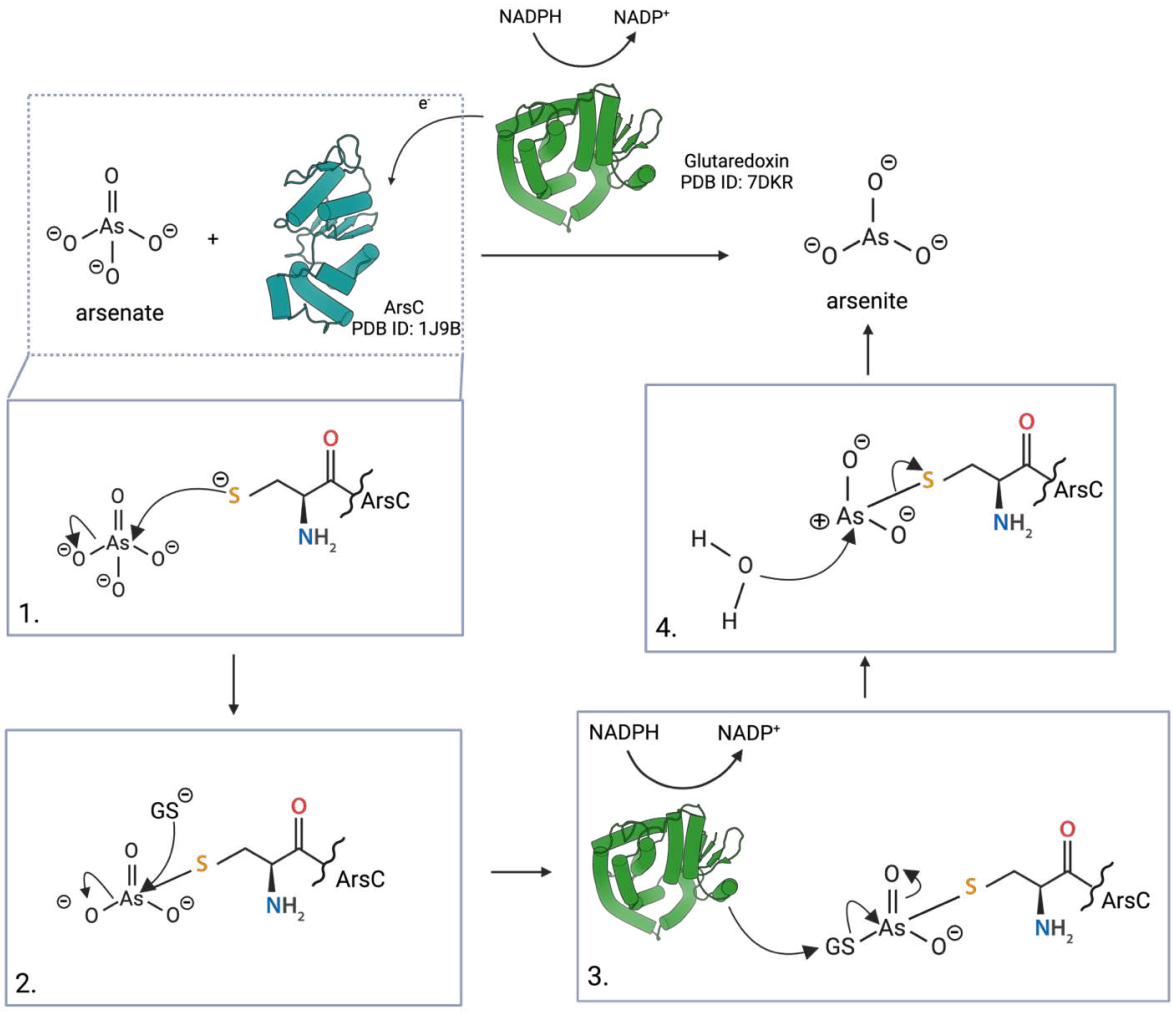

Figure 4: Predicted mechanism of ArsC reducing arsenate to arsenite in the presence of glutaredoxin2 as an electron donor. (1) ArsC and arsenate binding together via a nucleophilic attack (2) free glutathione attaches to enzyme-substrate complex (3) reduced glutaredoxin2 grabs the bound thiol group (4) protonation leads to the formation of arsenite

Arsenate has a standard reduction potential of +0.575 volts while arsenite has a +0.275 volt reduction potential.[38] A lower standard reduction potential indicates the species is less likely to undergo a reduction. This is consistent with a molecular docking study which found that arsenite has a low binding affinity to ArsC, likely due to the flexible active site.[30] The flexibility suggests that it could bind with other small molecules with similar chemical and structural properties. Given the structural similarities as well as similar reduction potentials between arsenite and $Bi(GSH)_3$ (i.e., standard reduction potential of $Bi(GSH)_3$ is +0.308), I hypothesized that ArsC could reduce $Bi(GSH)_3$ to an elemental bismuth.[38]

2.3 Identify ArsC's capability to reduce bismuth

Bismuth is located two rows below arsenic on the periodic table, and it shares similar chemical properties with other pnictogens. Trivalent $Bi(GSH)_3$ has a trigonal pyramidal geometry with three coordinating ligands, closely resembling arsenite's structure in terms of the number of coordinating ligands, oxidization state, geometry, as well as reduction potentials. Since $Bi(GSH)_3$ exhibits a strong affinity toward thiols, I hypothesize that the bismuth nanoparticles will be capped with glutathione controlling the size of the nanoparticle.[1]

For the reduction of bismuth(III) to bismuth(0) this reduction occurs via three electron transfers. Compared to the native reduction (arsenate to arsenite), an additional electron transfer occurs which could occur if the reduction is done subsequentially.

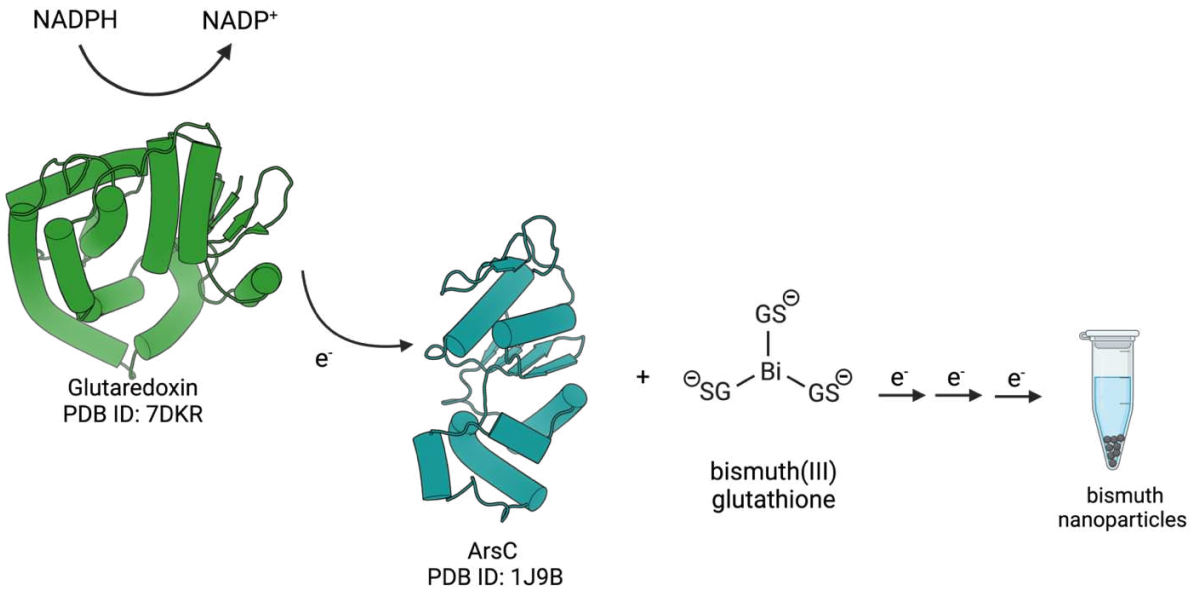

Figure 5: Proposed scheme of ArsC reducing bismuth(III) glutathione to bismuth(0) nanoparticle via three electron transfer

2.3.1 Determine Whether ArsC has Activity Towards a $Bi(GSH)_3$ Reduction

To assess whether ArsC has any native capability to reduce $Bi(GSH)_3$, enzymatic activity assays were designed to monitor the change in NADPH. NADPH assays are commonly used to evaluate redox reactions since an electron is required for the reaction to occur. This allows indirect tracking of the oxidation of NADPH, which can be measured spectrophotometrically. NADPH absorbs light at 340 nm, while its oxidized state ($NADP^+$) does not. A decrease in absorbance at 340 nm indicates NADPH oxidized, suggesting the redox reaction occurs.

NADPH serves as an enzymatic cofactor, starting the reaction by donating an electron to glutaredoxin2, which is an essential for the subsequent steps in the proposed mechanism. A decrease in the absorbance indicates NADPH oxidated to $NADP^+$, evidence that the enzymatic redox reaction occurs.

2.3.1.1 Results of ArsC Activity

The absorbance of NADPH was initially used to evaluate whether ArsC exhibited enzymatic activity towards $Bi(GSH)_3$ (synthesis in Appendix A). However, $Bi(GSH)_3$ and NADPH both absorb at 340 nm, resulting in a signal interference that prevented accurate tracking of NADPH oxidation (Figure 6A). To overcome this overlap, the assay was modified to use fluorescence. Here, an alternative wavelength of 450 nm was used to detect the emission of NADPH when excited at 340 nm. NADPH fluoresces at approximately 460 ± 60 nm, whereas $Bi(GSH)_3$ is not fluorescent, effectively eliminating the signal interference (Figure 6B).[40]

Even at high concentration of $Bi(GSH)_3$ (30 mM), there was minimal background signal, providing a higher sensitivity method in tracking NADPH oxidation. Control experiments suggest none of the other components (glutaredoxin2 and ArsC) in the assay exhibited fluorescence at 450 nm. This method provides an accurate way of tracking the change in NADPH over time (Figure 7).

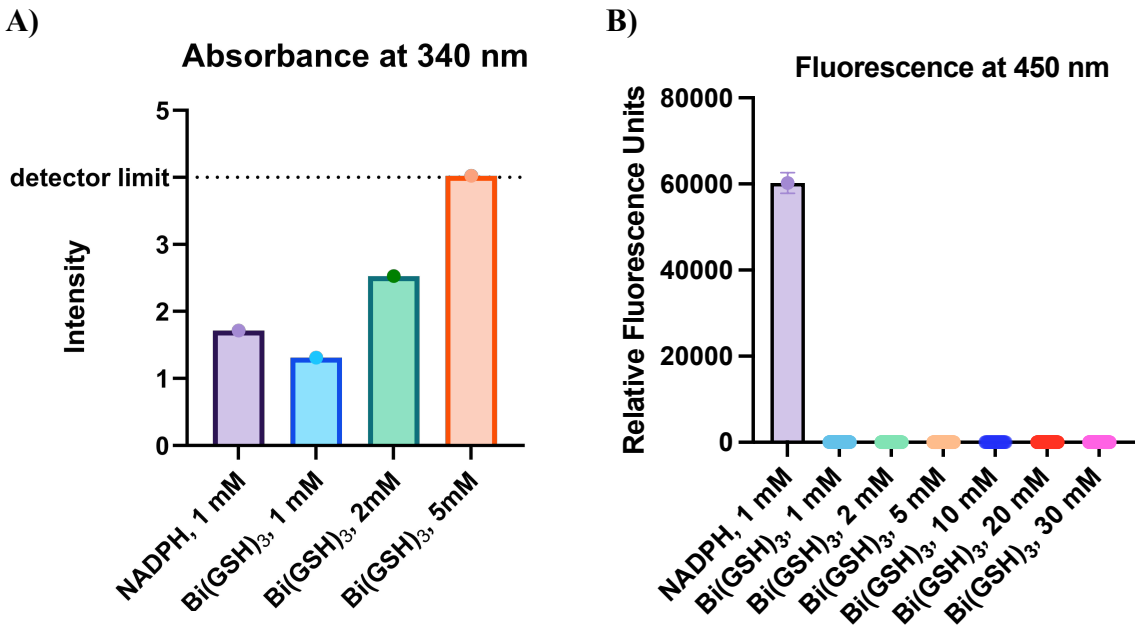

Figure 6: Absorbance and fluorescence based NADPH assays observing NADPH compared to various concentrations of $Bi(GSH)_3$ to assess signal interference A) $Bi(GSH)_3$ and NADPH show overlapping absorbance at 340 nm. B) NADPH fluoresces at 450 nm while $Bi(GSH)_3$ does not fluoresce.

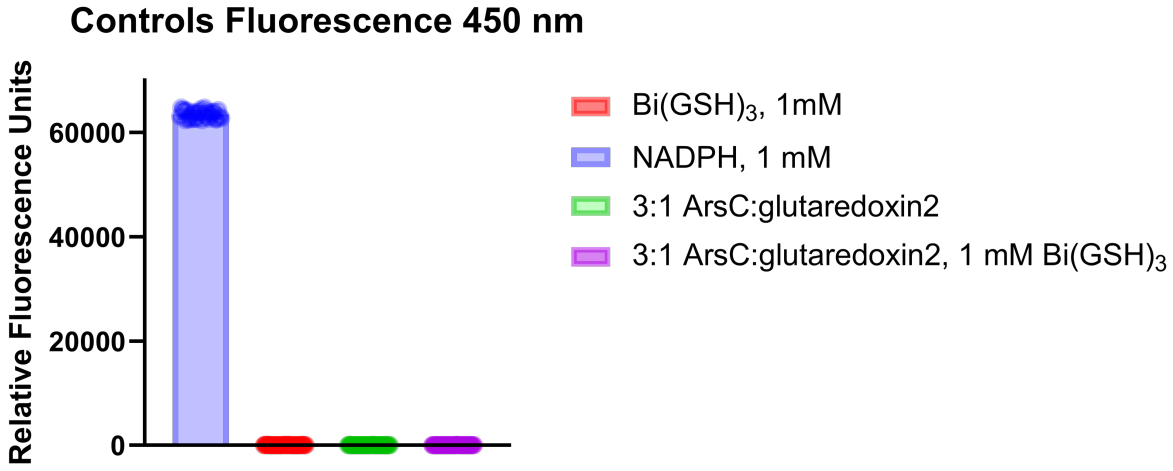

Figure 7: Fluorescence at 450 nm testing NADPH compared to the other components present in the assay. 3:1 ArsC:glutatredoxin2 and $Bi(GSH)_3$. NADPH exhibited fluorescence at 450 nm while ArsC, glutaredoxin2, and 1 mM $Bi(GSH)_3$ did not exhibit fluorescence.

NADPH emits fluorescence at 450 nm. A decrease in the fluorescence indicates the oxidization to $NADP^+$. When NADPH was added to the reaction mixture containing a 3:1 molar ratio of ArsC:glutaredoxin2 and 1 mM $Bi(GSH)_3$, a decrease in fluorescence was observed

(Figure 8). The 3:1 molar ratio of ArsC:glutaredoxin2 was selected based on the assumption that glutaredoxin2 can be regenerated by NADPH, allowing it to participate in multiple catalytic cycles. The observed decrease in fluorescence indicates NADPH being oxidized supporting the occurrence of the redox reaction. The enzymatic data supports the hypothesis that ArsC can reduce $Bi(GSH)_3$.

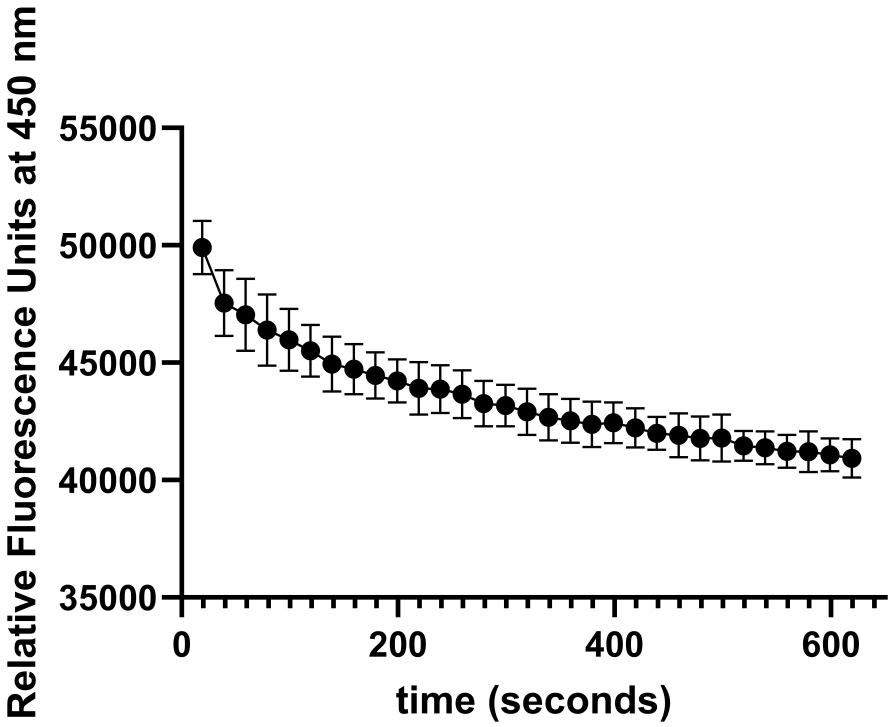

Figure 8: NADPH depletion assay using excitation at 340 nm and an excitation of 450 nm. A 3:1 ArsC:glutaredoxin2 ratio was used as well as 1 mM $Bi(GSH)_3$ and 1 mM NADPH.

Normally to quantify the amount of NADPH oxidized for spectrophotometry, Beer-Lambert's law is used (Appendix B). This law has a proportional relationship between the absorbance and the concentration of NADPH. Because fluorescence was used to track NADPH this equation will not work. Instead, a standard NADPH curve was used to correlate the relative fluorescence units to the concentration of NADPH (Figure 9A). The standard curve shows a linear trendline with a $R^2 = 0.9794$ (i.e., coefficient of determination), indicating there is a proportional relationship between the concentration of NADPH and the fluorescence. Running a

time trial to observe the NADPH does not spontaneously oxidize or reduce on its own. The slope from the standard curve was used to calculate the NADPH consumed (Equation 1). The calculations were done by subtracting the initial relative fluorescence units observed at ten seconds from the final relative fluorescent units at 600 seconds, using the linear equation to solve for the concentration of NADPH consumed (Figure 9A, Equation 1). ArsC was calculated to consume 16.00% NADPH over 600 seconds (Figure 9B). Although the observed NADPH oxidization was relatively low, this indicated ArsC exhibits some enzymatic activity toward $Bi(GSH)_3$. With this in mind, ArsC is a suitable candidate for a bismuth cloneable nanoparticle. Now, directed evolution can be used to enhance the enzyme's activity for a bismuth reduction.

A)

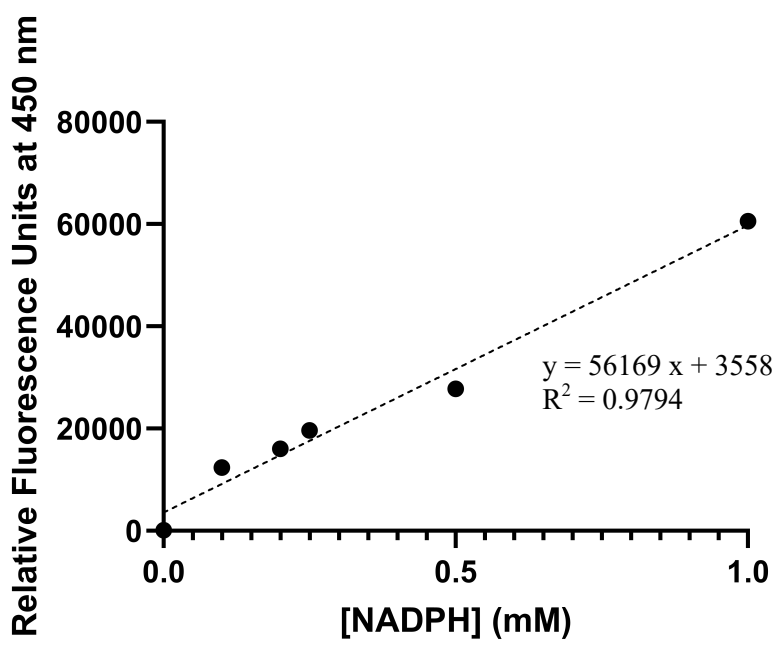

B)

$Bi(GSH)_3$ Substrate

	NADPH Oxidized
ArsC WT + glutaredxoin2	16.00%

Figure 9: A) NADPH standard curve using fluorescent at 450 nm B) Percentage of calculated NADPH oxidized during reactions.

$$y = mx + b$$

$$y = 56169\,x + 3558$$

Equation 1: Slope of NADPH standard curve (Figure 9). y is the change of the initial relative fluorescence units from the final relative fluorescent units, m is the change in relative fluorescence units over 600 seconds, x is the concentration of NADPH (mM), b is the relative fluorescent units with no NADPH present

Because NADPH must first be excited at 340 nm before it emits fluorescence, the initial fluorescence reading taken at ten seconds which may not reflect the precise initial fluorescence. In a future assay, the initial reading could be observed by removing glutaredoxin2 from the sample, based on the assumption that ArsC alone cannot reduce $Bi(GSH)_3$ without the electron transfer from glutaredoxin2. This will provide a more accurate NADPH consumption calculation.

Additionally, since the depletion curve did not fully plateau, this could suggest that further NADPH oxidation may have occurred. To improve the accuracy of consumed NADPH calculated extending the duration of the NADPH assays could prove better results. Additionally, kinetics studies could provide insight into the enzyme's affinity for the substrate (Michaelis constant, K_m), the rate at which substrate binds to the enzyme (turnover number), and the overall catalytic efficiency is the ratio of K_{cat}/K_m.

2.3.2 Using Analytical Techniques to Determine Bismuth Nanoparticles

Once enzymatic activity for $Bi(GSH)_3$ reduction was observed, analytical instruments were used to determine whether a nanoparticle formed. Based on the proposed mechanism of ArsC reducing $Bi(GSH)_3$, the expected product is an inorganic nanoparticle consisting of elemental bismuth (Figure 5). To evaluate particle formation *in vitro*, two analytical techniques were used (1) dynamic light scattering (DLS) and (2) transmission electron microscopy (TEM).

2.3.2.1 Determining Bismuth Nanoparticles Using DLS

DLS was used to measure the size distribution of particles in a solution.[41,42] This technique involves shining a laser beam through the sample to analyze fluctuations in the light scattering from random collisions, known as the Brownian motion. In the Brownian motion, the rate of fluctuation is directly related to the size of the particle, smaller particles travel faster while larger particles travel slower creating less fluctuations.[43] If the hypothesized product was formed, glutathione-capped bismuth nanoparticles, ideally a monodisperse peak (i.e., uniform particle size) would be expected since the capping agent regulates particle growth.[1] However, due to the presence of other components in the solution such as the proteins (ArsC and glutaredoxin2), additional peaks are expected.

2.3.2.2 Results Using DLS to Determine Bismuth Nanoparticles

Using the same conditions as the enzymatic activity assays (3:1 ArsC:glutaredoxin2 and 1 mM $Bi(GSH)_3$), DLS revealed a polydisperse peak ranging from 4000 nm to 6000 nm (Figure 10). The broad peak indicates a wide range of particles sizes which could be due to aggregation. Control DLS experiments observed a small peak around 5.5 nm corresponding to the proteins 3:1 ArsC:glutaredoxin2 (Appendix C). While the $Bi(GSH)_3$ control showed a peak of approximately 1.8 nm, likely attributed to salt in the buffer (phosphate buffer saline).

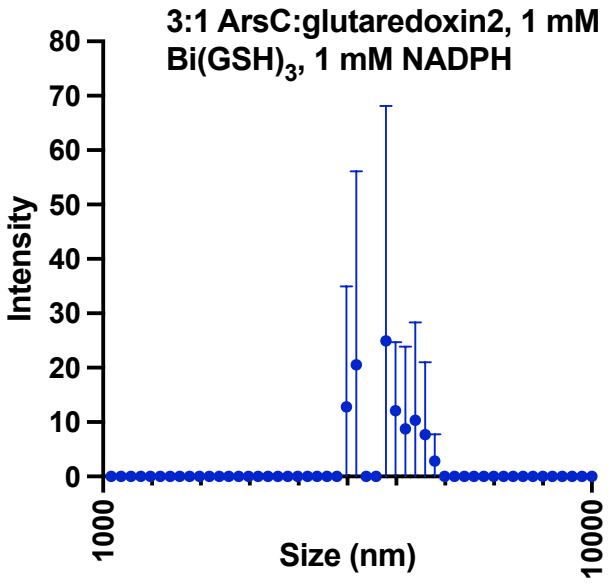

Figure 10: DLS used to verify bismuth nanoparticle formation using a 3:1 ArsC:glutaredoxin2, 1 mM Bi(GSH)3, and 1 mM NADPH. The broad peak ranging from 4000 to 6000 nm suggests aggregation.

To prevent protein aggregation, 1% glycerol in total volume was added to the solution. The 1% glycerol control showed no interference in DLS (Appendix C). To remove aggregation in the sample, centrifugation was performed in a stepwise manner with increasing speeds (5,000 rpm to 25,000 rpm).[44] After each step, the supernatant was collected and analyzed using DLS (Figure 11A). The first fraction (5,000 rpm) showed a reduced particle size around 500 -700 nm (seen in green Figure 11A). With increasing centrifugation speeds, particle size continued to decrease. The final fraction (labelled 5 centrifugation fraction), obtained at 25,000 rpm, had a monodisperse peak at approximately 4.5 – 7 nm (Figure 11A, Figure 11B). This peak likely reflects the nanoparticle and the proteins present since the protein controls were observed at 5.5 nm (Appendix C). While the centrifugation process improved the DLS measurements, the overlapping results with the protein controls makes it challenging to characterize the size of the bismuth particles. In future work, using a different analytical technique, such as Small-angle X-ray scattering could provide better insight into the particle size. This technique measures x-ray scattering at different angles to provide insight into the size of a particle.[45]

A)

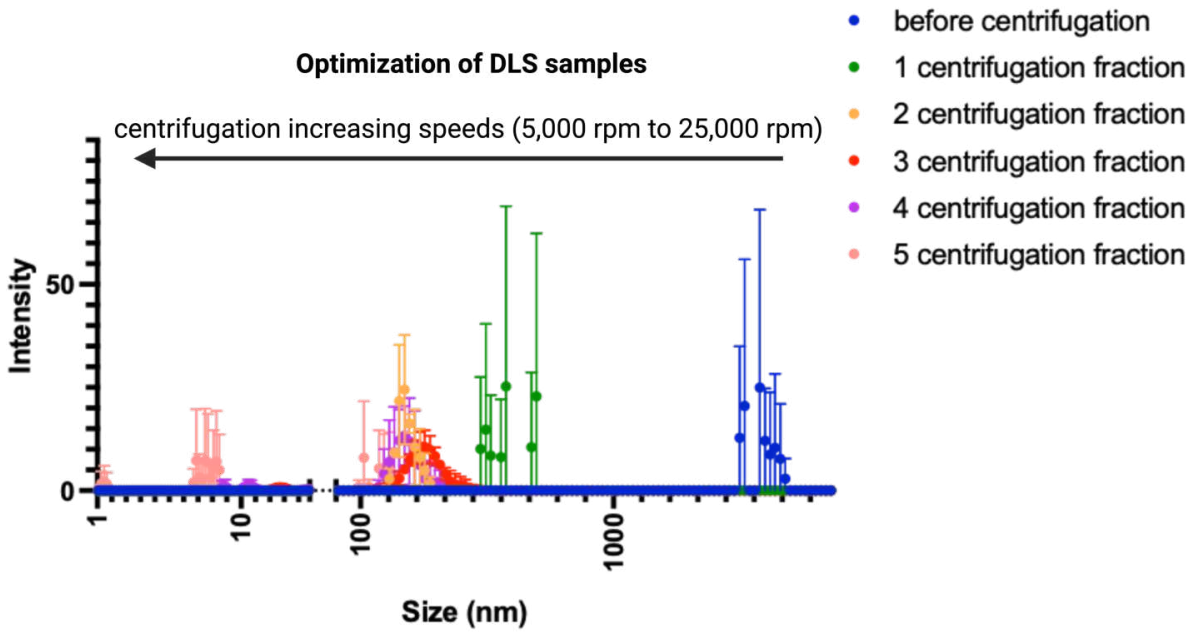

B)

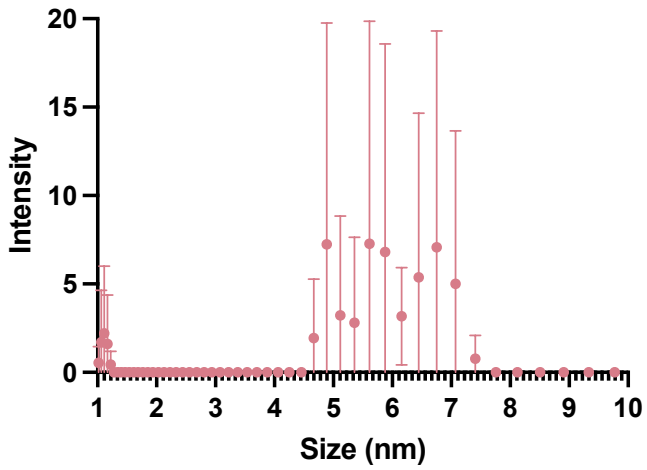

Figure 11: Optimization of DLS samples to observe bismuth nanoparticles A) using a centrifugation process with increasing speeds and fraction of each supernatant to remove large aggregates B) DLS of last fraction from centrifugation technique

2.3.2.4 Determining Bismuth Nanoparticles Using TEM

The enzymatic product was also examined using TEM to visualize the nanoparticle formation directly. In TEM, an electron beam is transmitted through the sample, while the

electron dense regions scatter electrons, preventing them from reaching the detector, this results in a darker area in the image.[46,47]

To further evaluate the particles, scanning transmission electron microscopy coupled with energy dispersive X-ray spectroscopy (STEM-EDS) was used to generate an elemental map that assigns chemical composition to each pixel in the image. STEM scans across the sample with an electron beam, exciting the atoms in the sample.[48] As the atoms relax back to a lower energy state, they emits energy specific to an individual element. EDS detects the emitted energy enabling identification of the specific elements.[48,49] While STEM provides spatial information, EDS offers elemental identification. Together the information can be overlayed to generate an elemental map that provides elemental detail across the sample surface.[48,49] Imaging was accomplished in collaboration with Tony Tien and Taylor Tomalinas.

2.3.2.5 Results of TEM Analysis of Bismuth Nanoparticles Formation

TEM imaging of the same enzymatic sample (3:1 ArsC:glutaredoxin2 and 1 mM $Bi(GSH)_3$) showed a small number of dark particles (seen in dark grey) along with a significant amount of aggregation, likely protein aggregation and salt crystals (Figure 12A).

The sample was rerun using the DLS centrifugation protocol to remove aggregation in the sample. TEM imaging of the last fraction (labelled 5 centrifugation fraction) revealed a small particle (diameter approximately 5.36 nm) with no visible aggregates (Figure 12B). This was consistent with the size observed from DLS. Very few particles were observed in TEM, which could be due to the low enzymatic activity. STEM-EDS determined the dark grey particles observed through TEM were composed of bismuth, supporting the hypothesis of ArsC reducing $Bi(GSH)_3$ into elemental bismuth nanoparticles (Appendix D Figure 19).

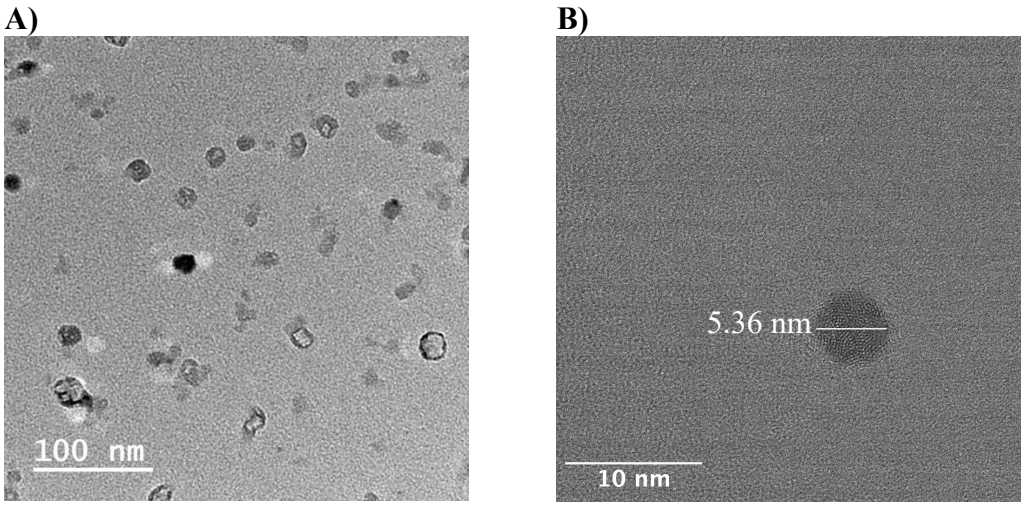

Figure 12: TEM of 3:1 ArsC:glutaredoxin2, 1 mM Bi(GSH)3, 1 mM NADPH. A) shows assays without any optimization showing large aggregation and salt crystals B) TEM image after centrifugation process removal of large aggregates.

Controls were run on TEM to verify no particles were formed without all of the components added (Appendix D Figure 18A-C). Further characterization of bismuth nanoparticles is necessary to determine the size of the particles. Due to the low number of particles observed in the TEM, running additional TEM samples could improve the analysis of particle distribution.

The enzymatic activity of ArsC reducing $Bi(GSH)_3$, combined with the evidence of particle formation, suggest ArsC is a promising candidate for directed evolution to improve its specificity and selectivity for $Bi(GSH)_3$ reduction.

CHAPTER 3: DIRECTED EVOLUTION OF ARSENATE REDUCTASE

3.1 Directed Evolution

In Chapter 2, ArsC exhibits potential enzymatic activity towards a $Bi(GSH)_3$ reduction, making it a good candidate for directed evolution. Error-prone polymerase chain reaction (epPCR) was used to generate a diverse library of ArsC variants.

Directed evolution is an accelerated strategy that mimic natural evolution to mutate a gene of interest and then identify an optimal variant with a desired function. For an enzyme to be improved through directed evolution, it must exhibit at least a minimal activity, which can then be improved through iterative rounds of mutagenesis and selection.[50]

Directed evolution is widely used in protein engineering because of its ability to optimize an enzyme without requiring structural, functional, or mechanistic knowledge.[51] This process involves introducing mutations in a gene of interest to generate a diverse pool of variants, known as a library. These variants are then evaluated for desired properties such as function, altered substrate specificity, thermostability, stability, activity.[52]

The first step in directed evolution is to generate a library of variants. One of the most widely used random mutagenesis techniques is epPCR due to its simplicity and robustness. The plasmid is fragmented using forward and reverse primes to a region of interest on the sequence, then epPCR introduces random mutations in the gene of interest by modifying the reaction conditions using a low-fidelity polymerase (specifically used mutazyme DNA polymerase) and the increasing magnesium ion concentration, which creates an unbalanced deoxynucleotide triphosphate balance.[53–55]

[1] I want to thank Rachel Cohen for the collaboration on the directed evolution of ArsC

Gibson Assembly was used to reassemble the mutated gene into a functional plasmid. This method takes the linearized fragments from the epPCR and ligates the fragments back together without the need for restriction enzymes. Instead, Gibson Assembly uses overlapping regions which are complementary to the adjacent fragment allowing then to anneal in that location.[56] Once a diverse library is generated, the variants are cloned into an expression vector.

The second step in directed evolution involves analyzing the variants through screening or selection. Screening assesses each individual variant to determine which variant exhibits a desired improved property; this process is time-consuming but an effective method.[57] In contrast, selection applies a specific growth condition that only functional or improved variants to survive, eliminating the nonfunction variants.[58] Selection process can significantly reduce the number of variants that need to be analyzed. However, a key challenge for this process is designing the specific growth conditions that reflect and select for the improved variants.

3.1.1 Results from Generating an ArsC Library Using Directed Evolution

epPCR was used to generate a diverse library of ArsC variants. In ArsC wild-type (WT) plasmid, the template backbone was cut using forward and reverse primers (plasmid map and primers in Appendix E) and run through polymerase chain reaction (PCR) using high-fidelity polymerase to amplify the backbone template without causing mutations to occur (Figure 13). The ArsC WT plasmid was also used to cut the ArsC gene using forward and reverse primers (primers in Appendix E) with epPCR to generate mutations in the ArsC gene (Figure 13). The fragmented mutated ArsC gene and the fragmented template backbone were ligated together using Gibson Assembly (Figure 13). Once reassembled, the library was transformed (i.e., uptaken into naked DNA) in *E. coli* BL21 cells via heat shock. Colonies were sequenced to verify the presence of intended mutations. In the first library (labelled Library 3 in Figure 13),

three colonies were sequenced, all three colonies contained two residues changed in each sequence. For the second library (labelled Library 4 in Figure 13), two colonies were sequences: one exhibited two residue changes, while the second colony contained a frameshift insertion. A frameshift insertion occurs when an additional nucleotide is inserted into the DNA sequence altering the codon reading. Both libraries were successfully generated.

Only a small number of colonies were successfully transformed via heat shock. In the future, switching to electroporation could improve transfection efficiency.[59] This approach applies a high-voltage current to temporarily permeabilize the cell membrane, allowing DNA to enter the cell.

To further verify the correct reassembly of the fragments, the WT ArsC gene was cut using the same forward and reverse primers (primers in Appendix E) followed by PCR (using high-fidelity polymerase to prevent mutations from occurring) and reassembled to the template backbone using Gibson Assembly (Figure 13). Followed by transformation in BL21 cells and plated on luria broth (LB) agar plates (Figure 13). Two out of three colonies were WT ArsC plasmid, indicating the ligation process was mostly successful.

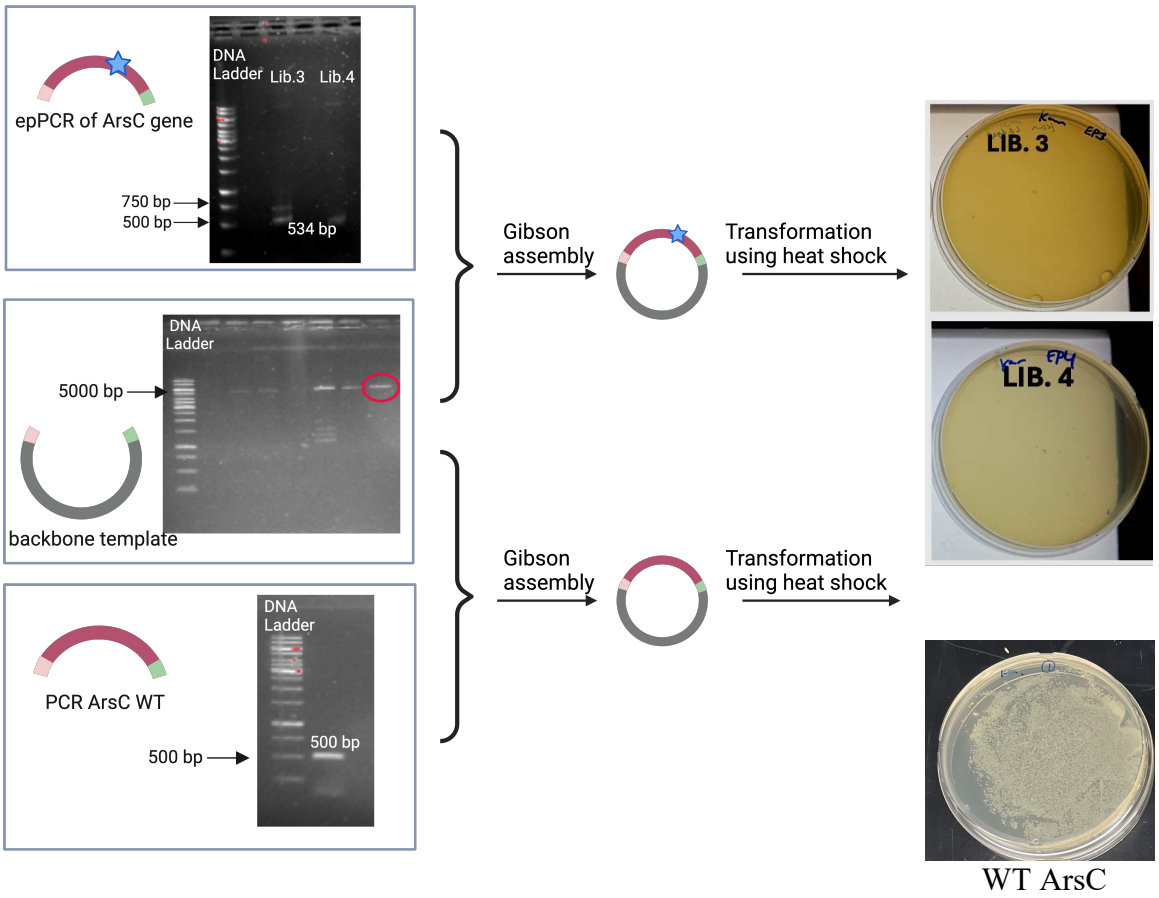

Figure 13: Schematic of generated ArsC library. Each lane shows different annealing temperatures to determine optimal conditions. First schematic: epPCR of ArsC gene creating a mutation (labelled Library 3 and Library 4) were ligated to backbone template (red circle was backbone used). Second schematic: PCR of WT ArsC (with no mutation) reassembling with backbone template to determine successful ligation of WT ArsC. Libraries 3 and 4 had a low number of colonies observed, making it challenging to image.

3.1.1.2 WT ArsC Tolerance to $Bi(GSH)_3$

Evaluating the tolerance of WT ArsC to $Bi(GSH)_3$ is essential for determining whether the variants in the library exhibit improved selectivity towards $Bi(GSH)_3$ reduction. Colony forming unit (CFU) assay were conducted to find a concentration of $Bi(GSH)_3$ that can be used to select the library.

CFU is a standard method for quantifying the viable microorganisms present in a specific condition.[60,61] This approach uses a serial dilution of a liquid culture, plating the diluted samples

onto an agar plate and counting the colonies that grow. CFU/mL is calculated (equation in Appendix F) to estimate the number of viable cells in a population, assuming each colony originates from a single viable bacteria cell.[60,62]

For accurate CFU estimations, colony counts should range from 30 to 300 per plate. Plates with colonies exceeding 300 may result in an underestimation due to overcrowding, while plates containing less than 30 colonies have a large standard deviation in the distribution.[60]

When investigating cell tolerance to metal exposure, it is important to establish a baseline of bacterial growth in the absence of metal. Which then can be compared to the change in cell viability when exposed to metal. As metal concentration increase, a decline in CFU is expected due to the metal toxicity killing the cells. The inhibitory concentration 90 (IC90) is defined as a decrease in 90% of the number of CFU on a plate, representing the threshold at which WT ArsC can no longer survive.

3.1.1.3 Results WT ArsC Tolerance to $Bi(GSH)_3$

CFU assays were performed to compare WT ArsC growth with varying concentrations of $Bi(GSH)_3$ to determine when $Bi(GSH)_3$ becomes toxic to ArsC WT.

Since glutathione is present in the $Bi(GSH)_3$ complex, it is important to account for how it may influence the growth of ArsC since glutathione protects cells against metal toxicity by maintaining redox balance.[11] By supplementing cultures with glutathione it could improve the metal tolerance.

WT ArsC grown without the presence of supplemented $Bi(GSH)_3$ or supplemented glutathione served as the baseline for colony formation (Figure 14). A 10-fold serial dilution was performed; to ensure the colonies count ranges from 30 – 300 colonies.

To separate the effects of bismuth from glutathione, cultures were exposed to either glutathione alone or an equivalent concentration of $Bi(GSH)_3$. CFU values were calculated for each concentration. These values were then used to calculate the growth ratio, which was achieved by dividing $Bi(GSH)_3$ colonies by the total number of colonies from both $Bi(GSH)_3$ and glutathione. This ratio was used to assess how bismuth affects ArsC WT growth.

The data showed no conclusive trend between the concentrations of 0.25 mM to 10 mM $Bi(GSH)_3$, which suggests that ArsC WT can tolerate those concentrations. However, at 30 mM $Bi(GSH)_3$, no colonies were observed. This concentration is toxic to WT ArsC and completely inhibits growth (Figure 14). The exact IC90 value remains unknown and requires further testing to establish the precise concentration at which $Bi(GSH)_3$ becomes toxic to WT ArsC, which can be used for the selection of the library.

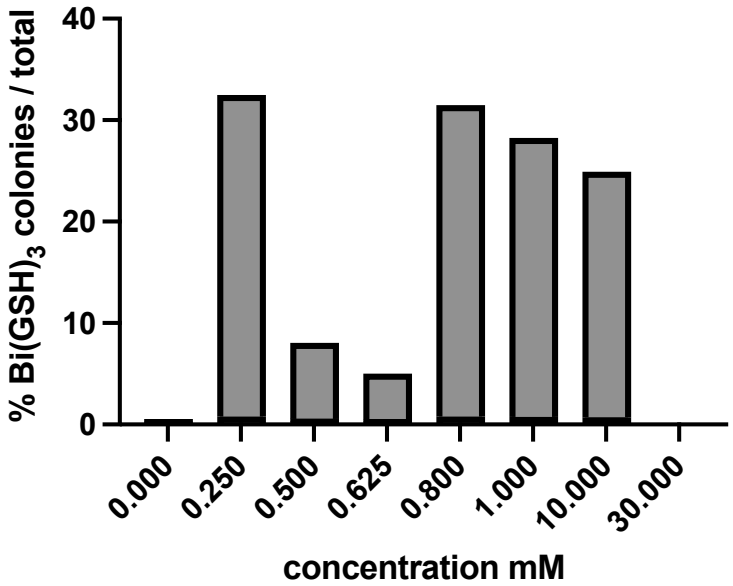

Figure 14: Percentage of $Bi(GSH)_3$ colonies /total. Total is the number of colonies observed from samples from $Bi(GSH)_3$ and glutathione added together to determine how increased concentration (mM) affects ArsC growth.

Due to inconclusive results observed between the 0.25 mM to 10 mM of $Bi(GSH)_3$ an alternative approach was done supplementing $Bi(GSH)_3$ into the LB agar plates instead of

supplementing into the culture. 2 mM $Bi(GSH)_3$ was selected since there appeared to be no decrease in cell growth between 1 mM to 10 mM $Bi(GSH)_3$.

When ArsC was plated onto 2 mM $Bi(GSH)_3$ supplemented into kanamycin agar plates, colonies grew (Figure 15). However, fewer colonies grew compared for the $Bi(GSH)_3$ supplemented plates compared to the plates without $Bi(GSH)_3$. This suggest 2 mM $Bi(GSH)_3$ is causing some level of stress in the cells. Additionally, 2 mM $Bi(GSH)_3$ combined with ITPG supplemented into kanamycin agar plates showed even less colony growth under these conditions. The decrease in the number of colonies observed for the bismuth supplemented plates compared to the plates without $Bi(GSH)_3$ suggests this concentration of $Bi(GSH)_3$ exhibited some level of toxic effect on the growth of ArsC WT. With this approach, using a serial dilution and varying the concentration of bismuth to find an IC90 value will be found.

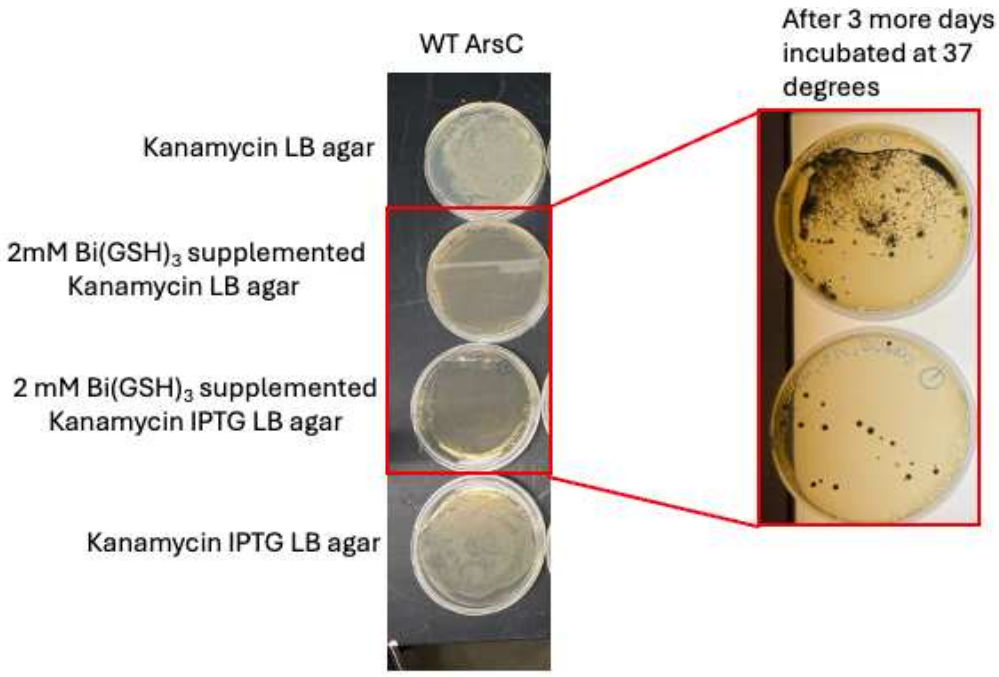

Figure 15: ArsC tolerance using $Bi(GSH)_3$ supplemented plates. 2 mM $Bi(GSH)_3$ supplemented plates were compared to controls. Plates were incubated at 37 degrees Celsius overnight, seen in left row, and were then incubated for an additional 3 days to observe black colonies.

To better understand $Bi(GSH)_3$ toxicity threshold, future work is required to analyze whether $Bi(GSH)_3$ successfully enters the cell and how much is uptaken into the cell. This can

provide a more accurate toxicity threshold. One method that could be considered is Inductively Coupled Plasma Mass Spectrometry, which is a widely used technique for quantifying elemental metal content in biological systems.[63,64,65]

3.1.2 Selection on the ArsC Library

The next step in the directed evolution experiment will be a selection of the library to determine which variants exhibit improved $Bi(GSH)_3$ reduction (Figure 16). Once an IC90 value is identified the library can be plated onto the corresponding concentration of $Bi(GSH)_3$ supplemented agar plates to observe which varies survive. The variants that survive under these conditions are assumed to exhibit an improved reduction of $Bi(GSH)_3$. Additionally, monitoring the time at which the colonies grow may provide insight into the $Bi(GSH)_3$ tolerance. With the assumption that variants that form colonies quicker may demonstrate a higher tolerance to $Bi(GSH)_3$.

The colonies that survive will be analyzed using fluorescence based NADPH assays to assess enzymatic activity toward $Bi(GSH)_3$.

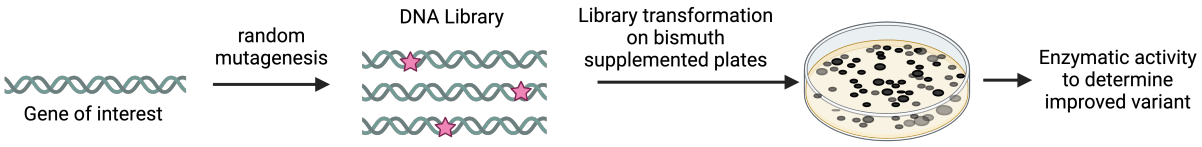

Figure 16: Directed evolution steps for mutation of ArsC WT. A library was created with random mutation using epPCR. The library will then be selected by plating variants onto bismuth supplemented plates to determine which variants survive. Enzymatic activity will be tested for the variants that survive.

CONCLUDING REMARKS

The overarching goal of this project was to develop bismuth cloneable nanoparticle, which are highly electron dense providing more contrast between the protein of interest and the background. Establishing this additional cloneable nanoparticles can create a platform of contrast markers which can be used in labelling of multiple proteins of interest within one cell.

My research focused on identifying a reductase capable of reducing $Bi(GSH)_3$ with the hypothesis to form a zerovalent bismuth nanoparticle. ArsC has shown promising preliminary enzymatic activity towards a bismuth reduction. Using directed evolution, random mutagenesis was used on the enzyme with the goal to identify an improve variant which exhibits higher substrate specificity for $Bi(GSH)_3$.

Throughout this project, I focused on optimizing assays to detect and quantify enzymatic activity and characterize $Bi(GSH)_3$ nanoparticle. These tools and findings will be helpful in the selection of variants from the directed evolution library and may also inform a broader application for other nanoparticles.

SUPPLEMENTARY

Appendix A:

$Bi(GSH)_3$ was made with a 3:1 molar ratio of bismuth(III) nitrate pentahydrate: reduced L-glutathione. Glutathione was dissolved in a 1X phosphate buffer saline buffer, then the addition of bismuth(III) nitrate pentahydrate was added and stirred until fully dissolved. Upon the addition of bismuth(III) nitrate pentahydrate, the solution turned an opaque yellow color, likely due to the poor solubility bismuth in water. The pH was adjusted to 7.4, which altered the shade of yellow but did not improve the solution transparency. After being left overnight, the solution became transparent, likely due to the formation of $Bi(GSH)_3$ complex. To confirm the structure, mass spectrometry should be used.

Although purification of this complex would be ideal for assays, there is limited research on this complex. Based on a similar complexes selenodiglutathione, a high pressure liquid chromatography machine is likely required for purification.[17]

Appendix B

Beer's Lambert Law looks at the change of light passing through the sample. The relationship between the absorbance and concentration of the sample are proportional making it possible to calculate the amount of NADPH consumed based on the absorbance.

$$A = \varepsilon bc$$

Equation 2: Beer's Lambert Law. A is the absorbance, ε is the molar absorptivity which known as a molar extension coefficient unique to the individual sample, b is the length of path, and c is the concentration.

Appendix C

DLS is used to measure the size distribution of particles. Controls were tested to observe the size of the proteins (Figure 17: Using DLS to verify bismuth nanoparticle formation. A) Protein and $Bi(GSH)_3$ *controls* were tested. B) controls to determine if 1% glycerol has an *overlapping* peak *with NADPH assay.* Optimization was done to see if aggregation could be removed from the sample. DLS control experiment of 1% glycerol in total solution compared to the final centrifugation fraction was tested to determine if there was interference between the peaks (Figure 17: Using DLS to verify bismuth nanoparticle formation. A) Protein and Bi(GSH)3 controls were tested. B) controls to determine if 1% glycerol has an overlapping peak with NADPH assay.

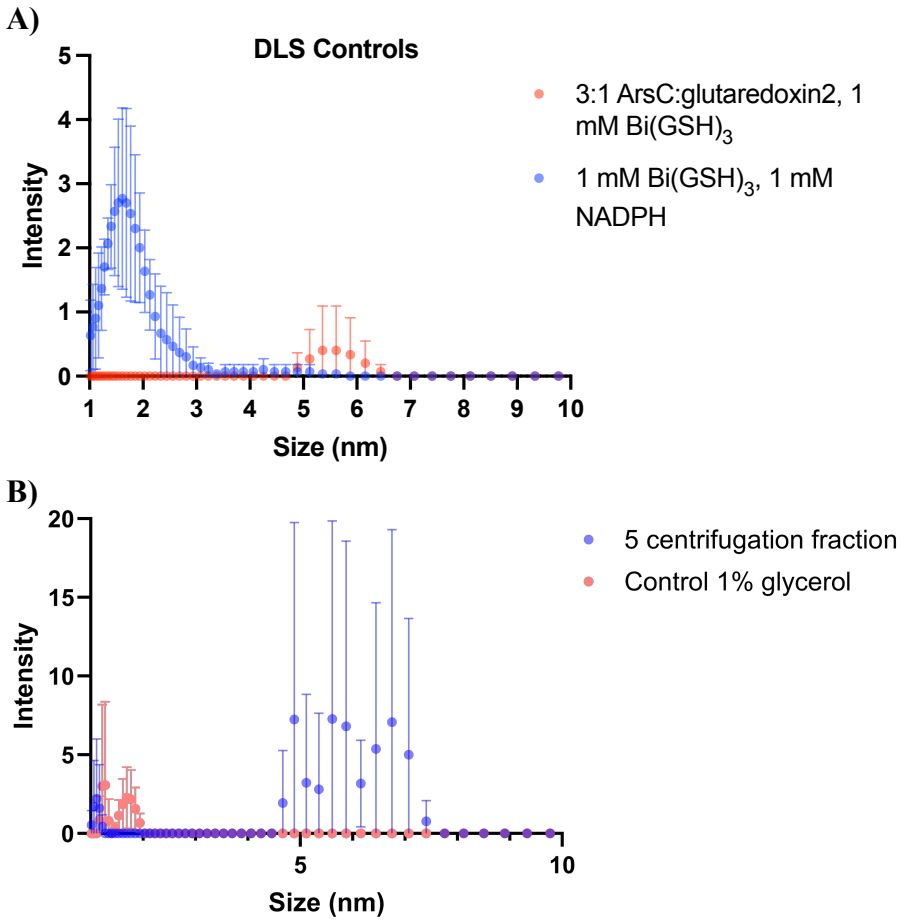

Figure 17: Using DLS to verify bismuth nanoparticle formation. A) Protein and $Bi(GSH)_3$ controls were tested. B) controls to determine if 1% glycerol has an overlapping peak with NADPH assay.

Appendix D

3:1 ArsC: glutaredoxin2 samples were run on TEM to observe if particle formation occurred (Figure 18). The only thing observed in the controls appeared to be salt crystals. Rerunning these controls at the same resolution would provide a better comparison of these samples.

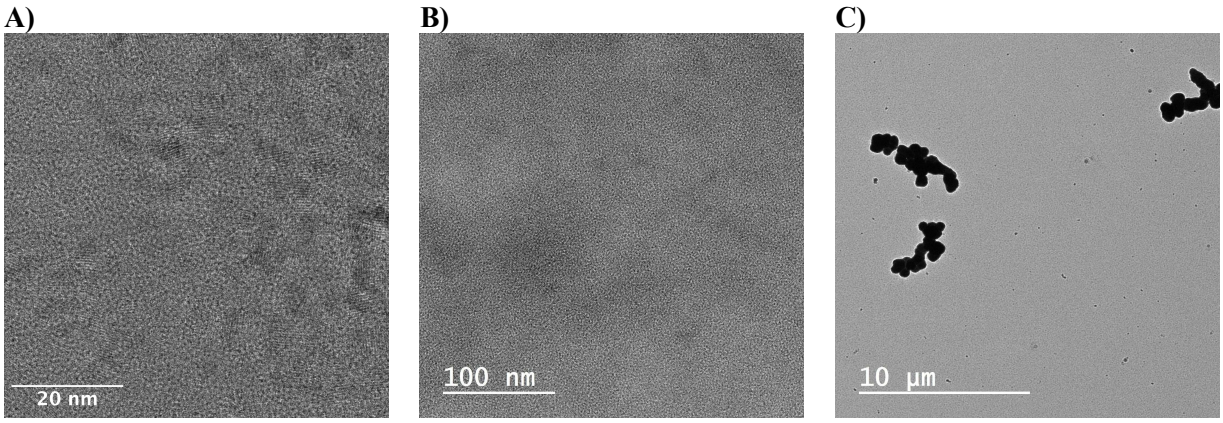

Figure 18: TEM controls. A) 1 mM $Bi(GSH)_3$ with NADPH. No particles were observed it appeared to have small aggregates present. B) 3:1 ArsC: glutaredoxin2 and NADPH. There were no particles observed on grid. C) 3:1 ArsC:glutaredoxin2 and 1 mM $Bi(GSH)_3$ no particles observed. It appeared to have salt aggregation which is observed.

STEM-EDS data was overlayed to provide an elemental map showing the chemical compositions present in every pixel of the image.

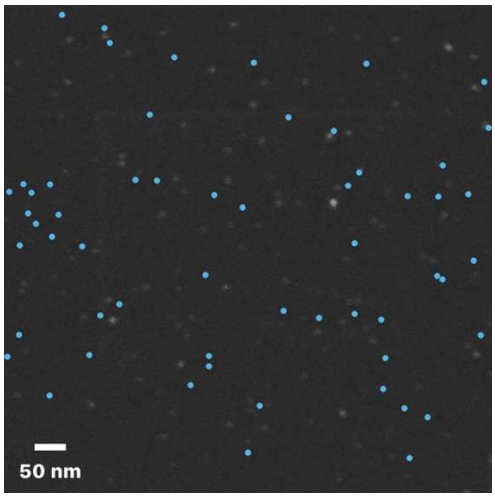

Figure 19: STEM-EDS data of centrifuged sample was run to determine chemical composition. White are electron dense areas on STEM and blue shows bismuth composition.

Appendix E

To cut the ArsC gene from the WT ArsC plasmid (pET29b+) forward and reverse primers were used. Additionally, the same process was conducted to cut the template backbone from ArsC plasmid.

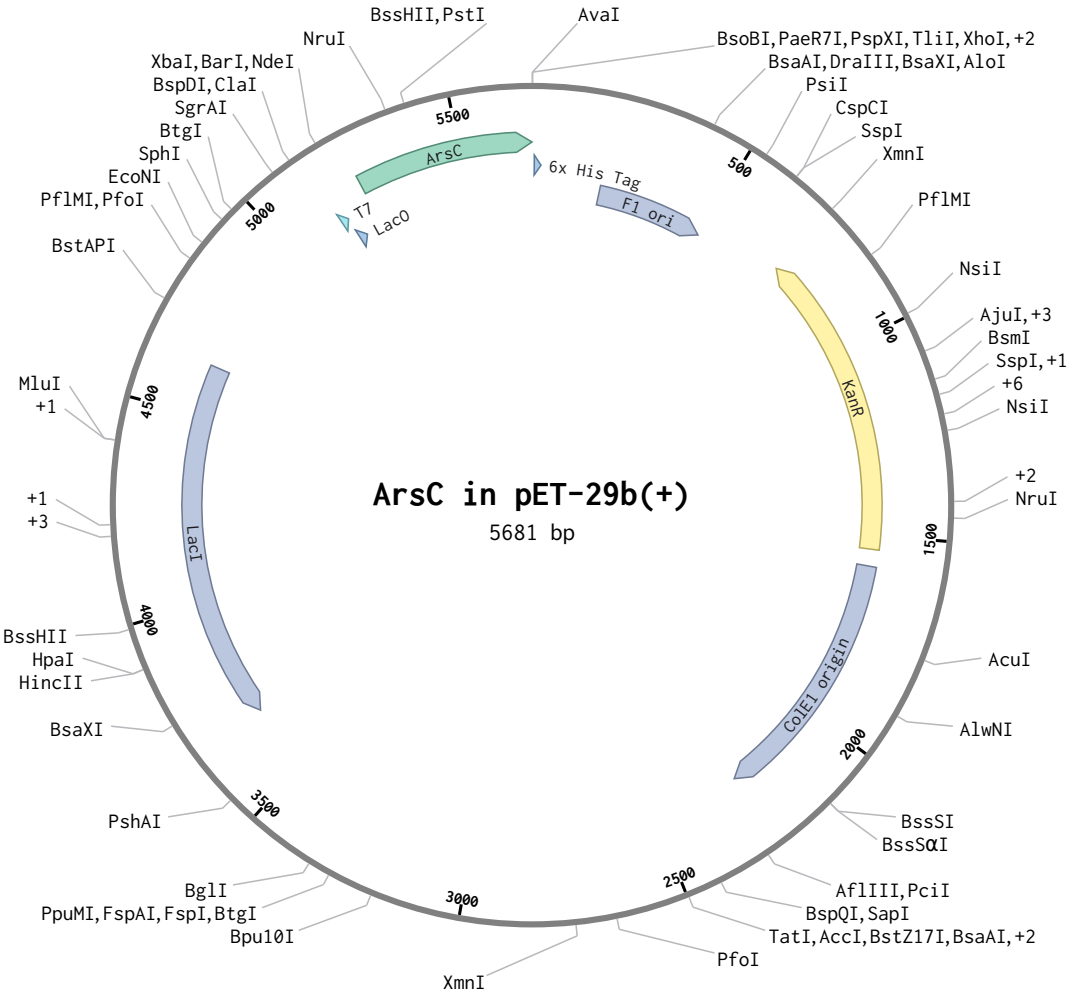

Figure 20: WT ArsC plasmid map in pET29b+. ArsC gene is seen in green.

Primers for template backbone:

Forwards primer: gctttgttagcagccggatc

Reverse primer: atgtatatctccttcttaaagttaaacaaaattatt

Primers for ArsC gene:

Forwards primer: tatatctccttcttaaagttaaacaaa

Reverse primer: ttcctttcgggctttgttagcagccgg

Appendix F

To calculate the number of colonies forming units can be used to quantifying the viable microorganisms present in a specific condition. A serial dilution of a liquid culture is generally plated onto an agar plate, then colonies are counted to quantify the viable cells in the population.

$$\frac{CFU}{mL} = \frac{(number\ of\ colonies)(Dilution\ factor)}{volume\ of\ culture\ plated\ (mL)}$$

Equation 3: Formula for calculating colony forming units (CFU/mL)

REFERENCES

(1) Borgognoni, K.; Guilliams, B.; Cohen, R.; Ackerson, C. Cloneable Selenium Nanoparticles As Multi-Modal Bio-Imaging Contrast Agents. ChemRxiv July 4, 2023. https://doi.org/10.26434/chemrxiv-2023-7sm53.

(2) Yuste, R. Fluorescence Microscopy Today. *Nat Methods* **2005**, *2* (12), 902–904. https://doi.org/10.1038/nmeth1205-902.

(3) Jensen, E. C. Types of Imaging, Part 2: An Overview of Fluorescence Microscopy. *The Anatomical Record* **2012**, *295* (10), 1621–1627. https://doi.org/10.1002/ar.22548.

(4) Huang, B.; Bates, M.; Zhuang, X. Super Resolution Fluorescence Microscopy. *Annu Rev Biochem* **2009**, *78*, 993–1016. https://doi.org/10.1146/annurev.biochem.77.061906.092014.

(5) Renz, M. Fluorescence Microscopy—A Historical and Technical Perspective. *Cytometry Part A* **2013**, *83* (9), 767–779. https://doi.org/10.1002/cyto.a.22295.

(6) Prakash, P. S.; Joshi, F. M.; Vogelsberg, E.; Cremers, G. A. O.; Gür, F. N.; Sato, Y.; de Greef, T. F. A.; Ader, M.; Kurth, T.; Nunes Gonçalves, D. P.; Schmidt, T. L. DNA Origami Barcodes for Immunostaining. *ACS Appl. Mater. Interfaces* **2025**, *17* (10), 15813–15823. https://doi.org/10.1021/acsami.4c19153.

(7) Vázquez-Gutiérrez, J. L.; Langton, M. Current Potential and Limitations of Immunolabeling in Cereal Grain Research. *Trends in Food Science & Technology* **2015**, *41* (2), 105–117. https://doi.org/10.1016/j.tifs.2014.10.002.

(8) Fung, H. K. H.; Hayashi, Y.; Salo, V. T.; Babenko, A.; Zagoriy, I.; Brunner, A.; Ellenberg, J.; Müller, C. W.; Cuylen-Haering, S.; Mahamid, J. Genetically Encoded Multimeric Tags for Subcellular Protein Localization in Cryo-EM. *Nat Methods* **2023**, *20* (12), 1900–1908. https://doi.org/10.1038/s41592-023-02053-0.

(9) Hendricks, A. R.; Cohen, R. S.; McEwen, G. A.; Tien, T.; Guilliams, B. F.; Alspach, A.; Snow, C. D.; Ackerson, C. J. Laboratory Evolution of Metalloid Reductase Substrate Recognition and Nanoparticle Product Size. *ACS Chem Biol* **2024**, *19* (2), 289–299. https://doi.org/10.1021/acschembio.3c00493.

(10) Lima de Silva, A. A.; de Carvalho, M. A. R.; de Souza, S. A. L.; Dias, P. M. T.; da Silva Filho, R. G.; de Meirelles Saramago, C. S.; de Melo Bento, C. A.; Hofer, E. Heavy Metal Tolerance (Cr, Ag AND Hg) in Bacteria Isolated from Sewage. *Braz J Microbiol* **2012**, *43* (4), 1620–1631. https://doi.org/10.1590/S1517-838220120004000047.

(11) Jozefczak, M.; Remans, T.; Vangronsveld, J.; Cuypers, A. Glutathione Is a Key Player in Metal-Induced Oxidative Stress Defenses. *International Journal of Molecular Sciences* **2012**, *13* (3), 3145–3175. https://doi.org/10.3390/ijms13033145.

(12) Bánfalvi, G. Heavy Metals, Trace Elements and Their Cellular Effects. In *Cellular Effects of Heavy Metals*; Banfalvi, G., Ed.; Springer Netherlands: Dordrecht, 2011; pp 3–28. https://doi.org/10.1007/978-94-007-0428-2_1.

(13) Hall, J. L. Cellular Mechanisms for Heavy Metal Detoxification and Tolerance.

(14) Hatfield, D. L.; Tsuji, P. A.; Carlson, B. A.; Gladyshev, V. N. Selenium and Selenocysteine: Roles in Cancer, Health and Development. *Trends Biochem Sci* **2014**, *39* (3), 112–120. https://doi.org/10.1016/j.tibs.2013.12.007.

(15) Kang, D.; Lee, J.; Wu, C.; Guo, X.; Lee, B. J.; Chun, J.-S.; Kim, J.-H. The Role of Selenium Metabolism and Selenoproteins in Cartilage Homeostasis and Arthropathies. *Exp Mol Med* **2020**, *52* (8), 1198–1208. https://doi.org/10.1038/s12276-020-0408-y.

(16) Sumner, S. E.; Markley, R. L.; Kirimanjeswara, G. S. Role of Selenoproteins in Bacterial Pathogenesis. *Biol Trace Elem Res* **2019**, *192* (1), 69–82. https://doi.org/10.1007/s12011-019-01877-2.
(17) Björnstedt, M.; Kumar, S.; Holmgren, A. Selenodiglutathione Is a Highly Efficient Oxidant of Reduced Thioredoxin and a Substrate for Mammalian Thioredoxin Reductase. *Journal of Biological Chemistry* **1992**, *267* (12), 8030–8034. https://doi.org/10.1016/S0021-9258(18)42403-9.
(18) Staicu, L. C.; Ackerson, C. J.; Cornelis, P.; Ye, L.; Berendsen, R. L.; Hunter, W. J.; Noblitt, S. D.; Henry, C. S.; Cappa, J. J.; Montenieri, R. L.; Wong, A. O.; Musilova, L.; Sura-de Jong, M.; van Hullebusch, E. D.; Lens, P. N. L.; Reynolds, R. J. B.; Pilon-Smits, E. a. H. Pseudomonas Moraviensis Subsp. Stanleyae, a Bacterial Endophyte of Hyperaccumulator Stanleya Pinnata, Is Capable of Efficient Selenite Reduction to Elemental Selenium under Aerobic Conditions. *J Appl Microbiol* **2015**, *119* (2), 400–410. https://doi.org/10.1111/jam.12842.
(19) Butz, Z. J.; Borgognoni, K.; Nemeth, R.; Nilsson, Z. N.; Ackerson, C. J. Metalloid Reductase Activity Modified by a Fused Se0 Binding Peptide. *ACS Chem. Biol.* **2020**, *15* (7), 1987–1995. https://doi.org/10.1021/acschembio.0c00387.
(20) Nemeth, R.; Neubert, M.; Butz, Z. J.; Ni, T. W.; Ackerson, C. J. Metalloid Reductase of Pseudomonas Moravenis Stanleyae Conveys Nanoparticle Mediated Metalloid Tolerance. *ACS Omega* **2018**, *3* (11), 14902–14909. https://doi.org/10.1021/acsomega.8b00826.
(21) Arsenic, Antimony and Bismuth. In *Chemistry of the Elements*; Elsevier, 1997; pp 547–599. https://doi.org/10.1016/B978-0-7506-3365-9.50019-5.
(22) Jiao, L.; Li, Q.; Deng, J.; Okosi, N.; Xia, J.; Su, M. Nanocellulose Templated Growth of Ultra-Small Bismuth Nanoparticles for Enhanced Radiation Therapy. *Nanoscale* **2018**, *10* (14), 6751–6757. https://doi.org/10.1039/C7NR06462D.
(23) Rosário, J. dos S.; Moreira, F. H.; Rosa, L. H. F.; Guerra, W.; Silva-Caldeira, P. P. Biological Activities of Bismuth Compounds: An Overview of the New Findings and the Old Challenges Not Yet Overcome. *Molecules* **2023**, *28* (15), 5921. https://doi.org/10.3390/molecules28155921.
(24) Hong, Y.; Lai, Y.-T.; Chan, G. C.-F.; Sun, H. Glutathione and Multidrug Resistance Protein Transporter Mediate a Self-Propelled Disposal of Bismuth in Human Cells. *Proc Natl Acad Sci U S A* **2015**, *112* (11), 3211–3216. https://doi.org/10.1073/pnas.1421002112.
(25) Ghorbani, A.; Emamverdian, A.; Pehlivan, N.; Zargar, M.; Razavi, S. M.; Chen, M. Nano-Enabled Agrochemicals: Mitigating Heavy Metal Toxicity and Enhancing Crop Adaptability for Sustainable Crop Production. *Journal of Nanobiotechnology* **2024**, *22* (1), 91. https://doi.org/10.1186/s12951-024-02371-1.
(26) *Arsenic and Cancer Risk*. https://www.cancer.org/cancer/risk-prevention/chemicals/arsenic.html (accessed 2025-03-18).
(27) Saltikov, C. W.; Olson, B. H. Homology of Escherichia Coli R773 arsA, arsB, and arsC Genes in Arsenic-Resistant Bacteria Isolated from Raw Sewage and Arsenic-Enriched Creek Waters. *Appl Environ Microbiol* **2002**, *68* (1), 280–288. https://doi.org/10.1128/AEM.68.1.280-288.2002.
(28) Garbinski, L. D.; Rosen, B. P.; Chen, J. Pathways of Arsenic Uptake and Efflux. *Environ Int* **2019**, *126*, 585–597. https://doi.org/10.1016/j.envint.2019.02.058.
(29) *UniProt*. UniProt. https://www.uniprot.org/uniprotkb/P15905/entry (accessed 2025-03-11).

(30) Rahman, Md. S.; Hossain, Md. S.; Saha, S. K.; Rahman, S.; Sonne, C.; Kim, K.-H. Homology Modeling and Probable Active Site Cavity Prediction of Uncharacterized Arsenate Reductase in Bacterial Spp. *Appl Biochem Biotechnol* **2021**, *193* (1), 1–18. https://doi.org/10.1007/s12010-020-03392-w.
(31) DeMel, S.; Shi, J.; Martin, P.; Rosen, B. P.; Edwards, B. F. P. Arginine 60 in the ArsC Arsenate Reductase of E. Coli Plasmid R773 Determines the Chemical Nature of the Bound As(III) Product. *Protein Science* **2004**, *13* (9), 2330–2340. https://doi.org/10.1110/ps.04787204.
(32) Ji, G.; Silver, S. Reduction of Arsenate to Arsenite by the ArsC Protein of the Arsenic Resistance Operon of Staphylococcus Aureus Plasmid pI258. *Proc Natl Acad Sci U S A* **1992**, *89* (20), 9474–9478. https://doi.org/10.1073/pnas.89.20.9474.
(33) López-Maury, L.; Sánchez-Riego, A. M.; Reyes, J. C.; Florencio, F. J. The Glutathione/Glutaredoxin System Is Essential for Arsenate Reduction in Synechocystis Sp. Strain PCC 6803. *J Bacteriol* **2009**, *191* (11), 3534–3543. https://doi.org/10.1128/JB.01798-08.
(34) Shi, J.; Mukhopadhyay, R.; Rosen, B. P. Identification of a Triad of Arginine Residues in the Active Site of the ArsC Arsenate Reductase of Plasmid R773. *FEMS Microbiology Letters* **2003**, *227* (2), 295–301. https://doi.org/10.1016/S0378-1097(03)00695-5.
(35) Liang, Y.; Yan, Y.; Shi, L.; Wang, M.; Yuan, X.; Wang, S.; Ye, L.; Yan, Z. Molecular Basis of Thioredoxin-Dependent Arsenic Transformation in Methanogenic Archaea. *Environ. Sci. Technol.* **2025**, *59* (1), 443–453. https://doi.org/10.1021/acs.est.4c06611.
(36) Shi, J.; Vlamis-Gardikas, A.; Aslund, F.; Holmgren, A.; Rosen, B. P. Reactivity of Glutaredoxins 1, 2, and 3 from Escherichia Coli Shows That Glutaredoxin 2 Is the Primary Hydrogen Donor to ArsC-Catalyzed Arsenate Reduction. *J Biol Chem* **1999**, *274* (51), 36039–36042. https://doi.org/10.1074/jbc.274.51.36039.
(37) Messens, J.; Silver, S. Arsenate Reduction: Thiol Cascade Chemistry with Convergent Evolution. *Journal of Molecular Biology* **2006**, *362* (1), 1–17. https://doi.org/10.1016/j.jmb.2006.07.002.
(38) Bratsch, S. G. Standard Electrode Potentials and Temperature Coefficients in Water at 298.15 K. *Journal of Physical and Chemical Reference Data* **1989**, *18* (1), 1–21. https://doi.org/10.1063/1.555839.
(39) Sadler, P. J.; Sun, H.; Li, H. Bismuth(III) Complexes of the Tripeptide Glutathione (γ-L-Glu–L-Cys–Gly). *Chemistry – A European Journal* **1996**, *2* (6), 701–708. https://doi.org/10.1002/chem.19960020615.
(40) Blacker, T. S.; Mann, Z. F.; Gale, J. E.; Ziegler, M.; Bain, A. J.; Szabadkai, G.; Duchen, M. R. Separating NADH and NADPH Fluorescence in Live Cells and Tissues Using FLIM. *Nat Commun* **2014**, *5* (1), 3936. https://doi.org/10.1038/ncomms4936.
(41) *2.4: Dynamic Light Scattering*. Chemistry LibreTexts. https://chem.libretexts.org/Bookshelves/Analytical_Chemistry/Physical_Methods_in_Chemistry_and_Nano_Science_(Barron)/02%3A_Physical_and_Thermal_Analysis/2.04%3A_Dynamic_Light_Scattering (accessed 2025-02-05).
(42) Babick, F. Dynamic Light Scattering (DLS). In *Characterization of Nanoparticles*; Elsevier, 2020; pp 137–172. https://doi.org/10.1016/B978-0-12-814182-3.00010-9.
(43) *Understanding Dynamic Light Scattering Theory - Waters | Wyatt Technology*. https://www.wyatt.com/library/theory/dynamic-light-scattering-theory.html (accessed 2025-03-21).

(44) Robertson, J. D.; Rizzello, L.; Avila-Olias, M.; Gaitzsch, J.; Contini, C.; Magoń, M. S.; Renshaw, S. A.; Battaglia, G. Purification of Nanoparticles by Size and Shape. *Sci Rep* **2016**, *6*, 27494. https://doi.org/10.1038/srep27494.
(45) *SAXS | Small-Angle X-ray Scattering*. https://www.malvernpanalytical.com/en/products/technology/xray-analysis/xray-scattering/small-angle-x-ray-scattering (accessed 2025-03-21).
(46) *What Is An Electron Microscope? 4 Types Of EM - VacCoat*. https://vaccoat.com/blog/electron-microscope/ (accessed 2025-02-24).
(47) Ilitchev, A. *Transmission (TEM) vs. Scanning (SEM) Electron Microscopes: What's the Difference?* Advancing Materials. https://www.thermofisher.com/blog/materials/tem-vs-sem-whats-the-difference/ (accessed 2025-03-21).
(48) *Scanning Transmission Electron Microscopy | Nanoscience Instruments*. https://www.nanoscience.com/techniques/scanning-transmission-electron-microscopy/ (accessed 2025-03-23).
(49) *What is EDS? | Energy Dispersive X-Ray Spectroscopy*. https://www.bruker.com/en/landingpages/bna/technology/what-is-eds.html (accessed 2025-03-21).
(50) *Exploring protein fitness landscapes by directed evolution | Nature Reviews Molecular Cell Biology*. https://www.nature.com/articles/nrm2805 (accessed 2025-03-15).
(51) Cobb, R. E.; Sun, N.; Zhao, H. Directed Evolution as a Powerful Synthetic Biology Tool. *Methods* **2013**, *60* (1), 81–90. https://doi.org/10.1016/j.ymeth.2012.03.009.
(52) Arnold, F. H.; Georgiou, G. *Directed Enzyme Evolution*; Humana Press: New Jersey, 2003; Vol. 230. https://doi.org/10.1385/1592593968.
(53) Biles, B. D.; Connolly, B. A. Low-Fidelity Pyrococcus Furiosus DNA Polymerase Mutants Useful in Error-Prone PCR. *Nucleic Acids Res* **2004**, *32* (22), e176. https://doi.org/10.1093/nar/gnh174.
(54) GeneMorph II Random Mutagenesis Kit. https://www.chem-agilent.com/pdf/strata/200550.pdf.
(55) Sellés Vidal, L.; Isalan, M.; Heap, J. T.; Ledesma-Amaro, R. A Primer to Directed Evolution: Current Methodologies and Future Directions. *RSC Chem Biol 4* (4), 271–291. https://doi.org/10.1039/d2cb00231k.
(56) Avilan, L. Assembling Multiple Fragments: The Gibson Assembly. *Methods Mol Biol* **2023**, *2633*, 45–53. https://doi.org/10.1007/978-1-0716-3004-4_4.
(57) Gupta, R. D.; Tawfik, D. S. Directed Enzyme Evolution via Small and Effective Neutral Drift Libraries. *Nat Methods* **2008**, *5* (11), 939–942. https://doi.org/10.1038/nmeth.1262.
(58) Stroik, S. *Plasmids 101: Screens vs. Selections*. https://blog.addgene.org/plasmid-101-screens-vs.-selections (accessed 2025-03-15).
(59) Lessard, J. C. Transformation of *E. Coli* Via Electroporation. In *Methods in Enzymology*; Lorsch, J., Ed.; Laboratory Methods in Enzymology: DNA; Academic Press, 2013; Vol. 529, pp 321–327. https://doi.org/10.1016/B978-0-12-418687-3.00027-6.
(60) Sieuwerts, S.; De Bok, F. A. M.; Mols, E.; De Vos, W. M.; Van Hylckama Vlieg, J. E. T. A Simple and Fast Method for Determining Colony Forming Units. *Letters in Applied Microbiology* **2008**, *47* (4), 275–278. https://doi.org/10.1111/j.1472-765X.2008.02417.x.
(61) Houchmandzadeh, B.; Ballet, P. A Novel Procedure for CFU Plating and Counting. *Journal of Microbiological Methods* **2023**, *206*, 106693. https://doi.org/10.1016/j.mimet.2023.106693.

(62) Brugger, S. D.; Baumberger, C.; Jost, M.; Jenni, W.; Brugger, U.; Mühlemann, K. Automated Counting of Bacterial Colony Forming Units on Agar Plates. *PLoS One* **2012**, *7* (3), e33695. https://doi.org/10.1371/journal.pone.0033695.
(63) Tsang, C.-N.; Ho, K.-S.; Sun, H.; Chan, W.-T. Tracking Bismuth Antiulcer Drug Uptake in Single Helicobacter Pylori Cells. *J. Am. Chem. Soc.* **2011**, *133* (19), 7355–7357. https://doi.org/10.1021/ja2013278.
(64) Wang, H.; He, M.; Chen, B.; Hu, B. Advances in ICP-MS-Based Techniques for Trace Elements and Their Species Analysis in Cells. *Journal of Analytical Atomic Spectrometry* **2017**, *32* (9), 1650–1659. https://doi.org/10.1039/C6JA00414H.
(65) *What is ICP-MS? Principles & Technique | Agilent*. https://www.agilent.com/en/product/atomic-spectroscopy/inductively-coupled-plasma-mass-spectrometry-icp-ms/what-is-icp-ms-icp-ms-faqs (accessed 2025-02-28).